Perturbations of slowly rotating black holes: Massive vector fields in the Kerr metric

Paolo Pani, Vitor Cardoso, Leonardo Gualtieri, Emanuele Berti, and Akihiro Ishibashi

Phys. Rev. D **86**, 104017 — Published 6 November 2012

DOI: 10.1103/PhysRevD.86.104017

Perturbations of slowly rotating black holes: massive vector fields in the Kerr metric

Paolo Pani,[1,*] Vitor Cardoso,[1,2,†] Leonardo Gualtieri,[3,‡] Emanuele Berti,[2,4,§] and Akihiro Ishibashi[5,6,¶]

[1] *CENTRA, Departamento de Física, Instituto Superior Técnico, Universidade Técnica de Lisboa - UTL, Av. Rovisco Pais 1, 1049 Lisboa, Portugal.*
[2] *Department of Physics and Astronomy, The University of Mississippi, University, MS 38677, USA.*
[3] *Dipartimento di Fisica, Università di Roma "La Sapienza" & Sezione INFN Roma1, P.A. Moro 5, 00185, Roma, Italy.*
[4] *California Institute of Technology, Pasadena, CA 91109, USA*
[5] *Theory Center, Institute of Particle and Nuclear Studies, High Energy Accelerator Research Organization (KEK), Tsukuba, 305-0801, Japan*
[6] *Department of Physics, Kinki University, Higashi-Osaka 577-8502, Japan*

We discuss a general method to study linear perturbations of slowly rotating black holes which is valid for any perturbation field, and particularly advantageous when the field equations are not separable. As an illustration of the method we investigate massive vector (Proca) perturbations in the Kerr metric, which do not appear to be separable in the standard Teukolsky formalism. Working in a perturbative scheme, we discuss two important effects induced by rotation: a Zeeman-like shift of nonaxisymmetric quasinormal modes and bound states with different azimuthal number m, and the coupling between axial and polar modes with different multipolar index ℓ. We explicitly compute the perturbation equations up to second order in rotation, but in principle the method can be extended to any order. Working at first order in rotation we show that polar and axial Proca modes can be computed by solving two decoupled sets of equations, and we derive a single master equation describing axial perturbations of spin $s = 0$ and $s = \pm 1$. By extending the calculation to second order we can study the superradiant regime of Proca perturbations in a self-consistent way. For the first time we show that Proca fields around Kerr black holes exhibit a superradiant instability, which is significantly stronger than for massive scalar fields. Because of this instability, astrophysical observations of spinning black holes provide the tightest upper limit on the mass of the photon: $m_\gamma \lesssim 4 \times 10^{-20}$ eV under our most conservative assumptions. Spin measurements for the largest black holes could reduce this bound to $m_\gamma \lesssim 10^{-22}$ eV or lower.

PACS numbers: 04.40.Dg, 04.62.+v, 95.30.Sf

I. INTRODUCTION

Linear perturbations of black holes (BHs) play a major role in physics. Many astrophysical processes can be modeled as small deviations from analytically known BH backgrounds: for instance, perturbative calculations of quasinormal modes (QNMs) are useful to describe the late stages of compact binary mergers or gravitational collapse [1–5], and BH perturbation theory provides an accurate description of the general relativistic dynamics of extreme mass-ratio inspirals [6–8]. Even when the understanding of complex astrophysical phenomena requires numerical relativity, the set up of the numerical simulations and the interpretation of the results are easier when we can rely on prior perturbative knowledge of the problem (see e.g. [9, 10]).

Besides their interest in modeling gravitational-wave sources for present and future detectors in Einstein's theory and in various proposed extensions of general relativity, perturbative studies of BH dynamics are also relevant in the context of high-energy physics [11]. Perturbation theory can shed light on several open issues, such as the stability properties of BH spacetimes in higher dimensions and in asymptotically anti-de Sitter spacetimes. Within the gauge-gravity duality, some of the correlation functions and transport coefficients are related to the lowest order BH QNMs. In a semiclassical treatment of BH evaporation, the calculation of greybody factors (which may be of direct interest for ongoing experiments) relies heavily on our ability to understand wave scattering in rotating BH spacetimes.

BH perturbation theory is a useful tool to investigate issues in astrophysics and high-energy physics as long as the radial and angular parts of the perturbation equations are separable. This usually happens when the background spacetime has special symmetries. If separable, the perturbation equations in the frequency domain reduce to a system of ordinary differential equations (ODEs) [12]. Separability is the norm if the background spacetime is spherically symmetric. Teukolsky [13] discovered that a large class of perturbation equations is exceptionally separable in the Kerr metric, the underlying reason being that the Kerr spacetime is of type D in the Petrov classification. Separability is much more difficult to achieve in the Kerr-Newman metric [12] and in higher spacetime dimensions [14]. In the Kerr background, perturbations induced by massless fields with integer and

* paolo.pani@ist.utl.pt
† vitor.cardoso@ist.utl.pt
‡ Leonardo.Gualtieri@roma1.infn.it
§ berti@phy.olemiss.edu
¶ akihiro.ishibashi@kek.jp

half-integer spins (including Dirac and Rarita-Schwinger fields [12, 13, 15]) are all separable, but this does not seem to be possible for some classes of perturbations, such as massive vector (Proca) perturbations [16].

Here we discuss a general method to study linear perturbations of slowly rotating BH backgrounds that is particularly useful when the perturbation variables are not separable. The method is an extension of Kojima's work on perturbations of slowly rotating neutron stars [17–19]. Slowly rotating backgrounds are "close enough" to spherical symmetry that an approximate separation of the perturbation equations in radial and angular parts becomes possible. The field equations can be Fourier transformed in time and expanded in spherical harmonics and they reduce, in general, to a coupled system of ODEs. This approach can be seen as a two-parameter perturbative expansion [20], where the small parameters are the amplitude of the perturbation and the angular velocity of the background. The method we present can in principle be extended to any order in the rotation parameter; here we derive the perturbation equations explicitly up to second order.

To first order in rotation, the final system of coupled ODEs can be simplified by dropping terms that couple perturbations with different values of the harmonic indices. This is a surprisingly good approximation: extending previous arguments by Kojima [19], we show that the neglected coupling terms can affect the frequencies and damping times of the QNMs only at second or higher order in the rotation rate. We support the analytical argument by numerical results, showing that the modes computed with and without the coupling terms coincide to first order in the rotation rate. At second order in rotation, the coupling of perturbations with different harmonic indices cannot be neglected. However, a notion of "conserved quantum number" ℓ is preserved: perturbations with given parity and harmonic index ℓ are coupled with perturbations with opposite parity and harmonic indices $\ell \pm 1$, and with perturbations with the same parity and harmonic indices $\ell \pm 2$ [21].

The main limitation of the present approach is the slow-rotation approximation. Currently this is not a restriction in extensions of general relativity including quadratic curvature corrections, where rotating BH solutions are only known in the slow-rotation limit [22–26]. Furthermore, as we show in this paper, a slow-rotation approximation is sufficient to describe important effects, like the superradiant instability of massive fields around rotating BHs. While a second-order expansion is needed to describe superradiance *consistently*, even the first-order approximation provides accurate results well beyond the nominal region of validity of the approximation. Similar extrapolations have been used in the past to predict the existence and timescale of r-mode instabilities in the relativistic theory of stellar perturbations (see e.g. [27–30]), and it is not unreasonable to expect that some quantities computed in the small-rotation regime (e.g. reflection coefficients) can be safely extrapolated to higher spin values. For all these reasons we are confident that perturbative studies of slowly rotating BHs will further our understanding of several interesting open problems in astrophysics and high-energy physics.

As an interesting testing ground of the slow-rotation approximation, here we focus on massive vector (Proca) perturbations of slowly rotating Kerr BHs. It is well known that massive bosonic fields in rotating BH spacetimes can trigger superradiant instabilities [31–37]. For scalar fields the instability is well studied. It is regulated by the dimensionless parameter $M\mu$ (in units $G = c = 1$), where M is the BH mass and $m_s = \mu\hbar$ is the bosonic field mass[1], and it is strongest for maximally spinning BHs, when $M\mu \sim 1$. For a solar mass BH and a field of mass $m_s \sim 1$ eV the parameter $M\mu \sim 10^{10}$. In this case the instability is exponentially suppressed [38] and in many cases of astrophysical interest the instability timescale would be larger than the age of the universe. However, strong superradiant instabilities ($M\mu \sim 1$) can occur either for light primordial BHs which may have been produced in the early universe [39–41] or for ultralight exotic particles found in some extensions of the standard model, such as the "string axiverse" scenario [42, 43]. In this scenario, massive scalar fields with 10^{-33} eV $< m_s < 10^{-18}$ eV could play a key role in cosmological models. Superradiant instabilities may allow us to probe the existence of such ultralight bosonic fields by producing gaps in the mass-spin BH Regge spectrum [42, 43], by modifying the inspiral dynamics of compact binaries [37, 44, 45] or by inducing a "bosenova", i.e. collapse of the axion cloud (see e.g. [46–48]).

Similar instabilities are expected to occur for massive hidden $U(1)$ vector fields, which are also a generic feature of extensions of the standard model [49–52]. Massive vector perturbations of rotating BHs are expected to induce a superradiant instability, but an explicit demonstration of this effect has been lacking. While this problem has been widely studied for massive scalar fields [31–37], the case of massive vector fields is still uncharted territory; incursions in the topic seem to be restricted to nonrotating backgrounds [16, 53–55]. The main reason is that the Proca equation, which describes massive vector fields, does not seem to be separable in the Kerr background. In the slow-rotation approximation we can reduce the problem of finding QNMs to a tractable system of coupled ODEs, where polar perturbations with angular index ℓ are generically coupled to axial perturbations with index $\ell \pm 1$ (and viceversa).

In this paper we derive the Proca perturbation equations up to second order in rotation, and for the first time we show that rotating BHs are indeed unstable to massive vector perturbations in the superradiant regime. At first order in rotation, perturbations with a given parity and

[1] In this paper, with a slight abuse of notation, we will use μ for both the scalar field mass ($\mu = m_s/\hbar$) and the vector field mass ($\mu = m_v/\hbar$). The meaning should be clear from the context.

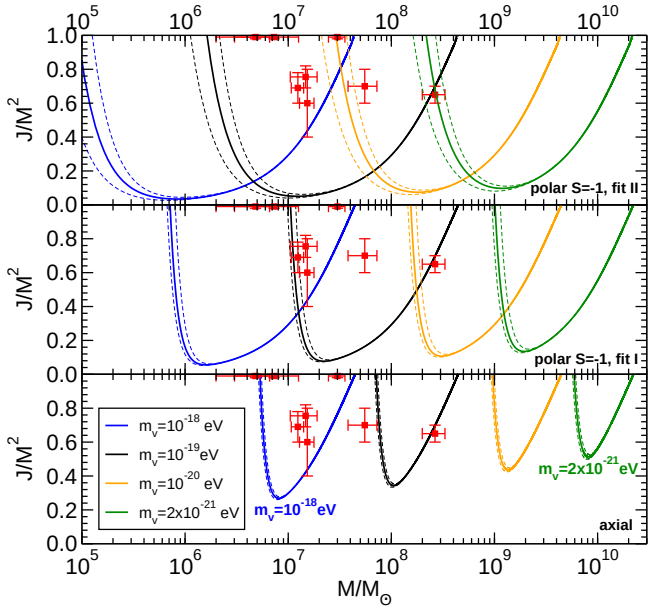

FIG. 1. (color online) Contour plots in the BH Regge plane [43] corresponding to an instability timescale shorter than a typical accretion timescale, $\tau_{\rm Salpeter} = 4.5 \times 10^7$ yr, for different values of the vector field mass $m_v = \mu\hbar$ (from left to right: $m_v = 10^{-18}$eV, 10^{-19}eV, 10^{-20}eV, 2×10^{-21}eV). For polar modes we consider the $S = -1$ polarization, which provides the strongest instability, and we use both Eq. (100) (fit II, top panel) and Eq. (95) (fit I, middle panel), and for axial modes we use Eq. (95) (bottom panel). Dashed lines bracket our estimated numerical errors. The experimental points (with error bars) refer to the mass and spin estimates of supermassive BHs listed in Table 2 of [56]; the rightmost point corresponds to the supermassive BH in Fairall 9 [57]. Supermassive BHs lying above each of these curves would be unstable on an observable timescale, and therefore they exclude a whole range of Proca field masses.

angular index ℓ are coupled to perturbations with $\ell \pm 1$ and opposite parity (cf. Eqs. (59), (60) and (61) below). However we show both analytically and numerically that this coupling does not affect the eigenfrequencies of the BH. In addition, the axial sector is described by a single master equation [Eq. (66) below], which is valid for both massive scalar and axial Proca perturbations. At second order in rotation the structure of the equations remain the same, but the $\ell \pm 1$ couplings do affect the eigenfrequency spectrum.

Quasinormal frequencies, damping times of stable modes and instability timescales of unstable modes in the slow-rotation limit can be computed using standard methods [4, 16, 35, 58]. As a test of our approximation scheme we revisit two problems for which "exact" solutions are known in the Kerr background. We study QNMs of massless vector perturbations to first order in rotation and we find that our slow-rotation method reproduces known results [4] with accuracy better than 1% when the dimensionless Kerr parameter $\tilde{a} = J/M^2 \lesssim 0.3$. In addition we compute stable and unstable *bound-state* modes (which are spatially localized within the vicinity of the BH and decay exponentially at spatial infinity [35]) of massive scalar perturbations up to second order in rotation, and we compare our results to the numerical calculations by Dolan [35]. We find good quantitative agreement with numerical results for nonsuperradiant frequencies, and we reproduce the imaginary part of superradiantly unstable modes within a factor 3 for $\tilde{a} \lesssim 0.7$, i.e. even for moderately large spin.

Extrapolations of our perturbative results indicate that, because of the strong superradiant instability of Proca perturbations, astrophysical BH spin measurements may set the most stringent bounds on the masses of vector fields [59]. This is shown in Fig. 1, where we summarize the astrophysical implications of our results (cf. Sect. VII for details). To be more specific, in Fig. 1 we show exclusion regions in the "BH Regge plane" (cf. Fig. 3 of [43]), i.e. we plot contours corresponding to an instability timescale of the order of a typical accretion timescale (the Salpeter time $\tau_{\rm Salpeter} = 4.5 \times 10^7$ yr) for four different masses of the Proca field ($m_v = 10^{-18}$ eV, 10^{-19} eV, 10^{-20} eV and 2×10^{-21} eV) and for axial modes (bottom panel) and polar modes (top and middle panels). For polar modes we consider only the $S = -1$ polarization, which provides the strongest instability (cf. Sec. (VI D) for details). While our numerical results for the axial modes are supported by an analytical formula, in the polar case we have used two different functions to fit the numerical data at second order in the BH spin. The plot shows that essentially *any* spin measurement for supermassive BHs with $10^6 M_\odot \lesssim M \lesssim 10^9 M_\odot$ would exclude a wide range of vector field masses.

The rest of the paper is organized as follows. In Sec. II we outline the general method, which is valid for any stationary and axisymmetric background and for any kind of perturbation. In Sec. III we study massive Klein-Gordon perturbations of slowly rotating Kerr BHs up to second order in rotation and outline how the method can be extended, at least in principle, to higher orders. In Sec. IV we specialize to Proca perturbations of slowly rotating Kerr BHs. In Sec. V we set up the eigenvalue problem for quasinormal modes and bound states, and in Sec. VI we present our numerical results. Section VII deals with the implications of the superradiant instability for astrophysics and fundamental physics. In Sec. VIII we draw some conclusions and we discuss possible future applications of the method. To improve readability we relegate some technical material to the appendices. Appendix A lists the coefficients appearing in the scalar and Proca perturbation equations. Appendix B shows explicitly the perturbation equations for a Proca field on a slowly rotating Kerr background to first order in rotation, and appendix C generalizes Detweiler's analytical calculation of the unstable massive scalar modes of a Kerr BH [60] to axial perturbations of a massive vector field up to linear order in rotation.

To reduce the risk of typographical errors and facilitate

comparison with our results, we made many of our calculations available online as *Mathematica* notebooks [61].

II. PERTURBATIONS OF A SLOWLY ROTATING BLACK HOLE: GENERAL METHOD

In this section we outline the strategy to study generic (scalar, vector, tensor, etcetera) perturbations of *any* stationary, axisymmetric background up to second order in the rotation parameter, but in principle the formalism can be extended to *any* order. We consider the most general stationary axisymmetric spacetime

$$ds_0^2 = -H^2 dt^2 + Q^2 dr^2 + r^2 K^2 \left[d\vartheta^2 + \sin^2\vartheta (d\varphi - L dt)^2\right] ,$$

where H, Q, K and L are functions of r and ϑ only. To second order, the metric above can be expanded as [62]

$$\begin{aligned} ds_0^2 =& -F(r)\left[1+F_2\right]dt^2 + B(r)^{-1}\left[1+\frac{2B_2}{r-2M}\right]dr^2 \\ &+ r^2(1+k_2)\left[d\vartheta^2 + \sin^2\vartheta(d\varphi - \varpi dt)^2\right] , \end{aligned} \tag{1}$$

where M is the mass of the spacetime, ϖ is a function of r linear in the rotation parameter, and F_2, B_2 and k_2 are functions of r and ϑ quadratic in the rotation parameter. Because H, K and Q all transform like scalars under rotation, they can be expanded in scalar spherical harmonics which, due to axisymmetry, reduce to the Legendre polynomials $P_\ell(\vartheta)$. As shown in Ref. [62], only $\ell = 0$ and $\ell = 2$ polynomials contribute at second order in rotation; therefore F_2 can be expressed as $F_2(r,\vartheta) = F_r(r) + F_\vartheta(r) P_2(\vartheta)$, and the same applies to $B_2(r,\vartheta)$ and $k_2(r,\vartheta)$.

At first order in rotation the background (1) can be written in the simpler form

$$\begin{aligned} ds_0^2 =& -F(r)dt^2 + B(r)^{-1}dr^2 + r^2 d^2\Omega \\ &- 2\varpi(r)\sin^2\vartheta d\varphi dt . \end{aligned} \tag{2}$$

Note that, given a nonrotating metric, the gyromagnetic function $\varpi(r)$ can be computed using the approach originally developed by Hartle [62]. For example, slowly rotating Kerr BHs [cf. Eq. (18) below] correspond to $F(r) = B(r) = 1 - 2M/r$ and $\varpi = 2M^2\tilde{a}/r$, where M and $J = M^2\tilde{a}$ are the mass and the angular momentum of the BH. Furthermore, the general metrics (1) and (2) encompass (among others) slowly rotating Kerr-Newman BHs and BH solutions in modified gravity theories; the latter have been derived analytically only up to first order [22, 25] (and more recently to second order [26]) in the BH spin.

Scalar, vector and tensor field equations in the background metric (1) can be linearized in the field perturbations (that we shall schematically denote by δX) as well as in the BH angular momentum. We neglect terms of second order in the perturbation amplitude δX and terms of third order in the rotation parameter $\tilde{a}$, Fourier transform the perturbations, and expand them in tensor spherical harmonics:

$$\delta X_{\mu_1\ldots}(t,r,\vartheta,\varphi) = \delta X^{(i)}_{\ell m}(r) \mathcal{Y}^{\ell m\,(i)}_{\mu_1\ldots} e^{-\mathrm{i}\,\omega t} , \tag{3}$$

where $\mathcal{Y}^{\ell m\,(i)}_{\mu_1\ldots}$ is a basis of scalar, vector or tensor harmonics (depending on the tensorial nature of the perturbation δX) and the frequency ω is, in general, complex. The perturbation variables $\delta X^{(i)}_{\ell m}(r)$ can be classified as "polar" or "axial" depending on their behavior under parity transformations ($\vartheta \to \pi - \vartheta$, $\varphi \to \varphi + \pi$): polar and axial perturbations are multiplied by $(-1)^\ell$ and $(-1)^{\ell+1}$, respectively.

With the introduction of the expansion (3), the linear response of the system is fully characterized by the quantities $\delta X^{(i)}_{\ell m}(r)$. The perturbation equations, expanded in spherical harmonics and Fourier transformed in time, yield a coupled system of ODEs in the perturbation functions $\delta X^{(i)}_{\ell m}(r)$. In the case of a spherically symmetric background, perturbations with different values of $(\ell,\, m)$, as well as perturbations with opposite parity, are decoupled. In a rotating, axially symmetric background, perturbations with different values of m are decoupled[2] but perturbations with different values of ℓ are not. However, in the limit of slow rotation there is a Laporte-like "selection rule" [21]: at first order in $\tilde{a}$, perturbations with a given value of ℓ are only coupled to those with $\ell \pm 1$ and *opposite* parity, similarly to the case of rotating stars. At second order, perturbations with a given value of ℓ are also coupled to those with $\ell \pm 2$ and *same* parity, and so on.

In general, the perturbation equations can be written in the following form:

$$\begin{aligned} 0 =& \mathcal{A}_\ell + \tilde{a} m \bar{\mathcal{A}}_\ell + \tilde{a}^2 \hat{\mathcal{A}}_\ell \\ &+ \tilde{a}(\mathcal{Q}_\ell \tilde{\mathcal{P}}_{\ell-1} + \mathcal{Q}_{\ell+1}\tilde{\mathcal{P}}_{\ell+1}) \\ &+ \tilde{a}^2\left[\mathcal{Q}_{\ell-1}\mathcal{Q}_\ell \breve{\mathcal{A}}_{\ell-2} + \mathcal{Q}_{\ell+2}\mathcal{Q}_{\ell+1}\breve{\mathcal{A}}_{\ell+2}\right] + \mathcal{O}(\tilde{a}^3) , \end{aligned} \tag{4}$$

$$\begin{aligned} 0 =& \mathcal{P}_\ell + \tilde{a} m \bar{\mathcal{P}}_\ell + \tilde{a}^2 \hat{\mathcal{P}}_\ell \\ &+ \tilde{a}(\mathcal{Q}_\ell \tilde{\mathcal{A}}_{\ell-1} + \mathcal{Q}_{\ell+1}\tilde{\mathcal{A}}_{\ell+1}) \\ &+ \tilde{a}^2\left[\mathcal{Q}_{\ell-1}\mathcal{Q}_\ell \breve{\mathcal{P}}_{\ell-2} + \mathcal{Q}_{\ell+2}\mathcal{Q}_{\ell+1}\breve{\mathcal{P}}_{\ell+2}\right] + \mathcal{O}(\tilde{a}^3) . \end{aligned} \tag{5}$$

Here

$$\mathcal{Q}_\ell = \sqrt{\frac{\ell^2 - m^2}{4\ell^2 - 1}} ; \tag{6}$$

$\mathcal{A}_\ell$, $\bar{\mathcal{A}}_\ell$, $\tilde{\mathcal{A}}_\ell$, $\hat{\mathcal{A}}_\ell$, $\breve{\mathcal{A}}_\ell$ are *linear* combinations of the axial perturbations and of their derivatives, with multipolar

[2] From now on we will append the relevant multipolar index ℓ to any perturbation variable but we will omit the index m, because in an axisymmetric background it is possible to decouple the perturbation equations so that all quantities have the same value of m.

index ℓ; similarly, $\mathcal{P}_\ell$, $\bar{\mathcal{P}}_\ell$, $\tilde{\mathcal{P}}_\ell$, $\hat{\mathcal{P}}_\ell$, $\breve{\mathcal{P}}_\ell$ are linear combinations of the polar perturbations and of their derivatives, with index ℓ. The dimensionless parameter $\tilde{a}$ keeps track of the order of the various terms in the slow-rotation expansion.

The structure of Eqs. (4)–(5) is the following. Perturbations with a given parity and index ℓ are coupled to: (i) perturbations with *opposite* parity and index $\ell \pm 1$ at order $\tilde{a}$; (ii) perturbations with *same* parity and *same* index ℓ up to order $\tilde{a}^2$; (iii) perturbations with *same* parity and index $\ell \pm 2$ at order $\tilde{a}^2$.

From Eq. (6) it follows that $\mathcal{Q}_{\pm m} = 0$, and therefore if $|m| = \ell$ the coupling of perturbations with index ℓ to perturbations with indices $\ell - 1$ and $\ell - 2$ is suppressed. Since the contribution $|m| = \ell$ dominates the linear response of the system, this general property of Eqs. (4)–(5) is reminiscent of a "propensity rule" in atomic theory, which states that transitions $\ell \to \ell + 1$ are strongly favored over transitions $\ell \to \ell - 1$ (cf. [21] and references therein).

Due to the coupling between different multipolar indices, the spectrum of the solutions of Eqs. (4)–(5) is extremely rich. However, if we are interested in the characteristic modes of the slowly rotating background to first or to second order in $\tilde{a}$, the perturbation equations can be considerably simplified. We discuss the truncation to first and to second order in the next two sections, respectively.

A. Eigenvalue spectrum to first order

Let us consider the first order expansion of Eqs. (4) and (5). We expand all quantities to first order and we ignore the terms $\hat{\mathcal{A}}_\ell$, $\breve{\mathcal{A}}_\ell$, $\hat{\mathcal{P}}_\ell$ and $\breve{\mathcal{P}}_\ell$, which are multiplied by $\tilde{a}^2$. Furthermore the terms ($\tilde{\mathcal{P}}_\ell$, $\tilde{\mathcal{A}}_\ell$) in Eqs. (4) and (5) do not contribute to the eigenfrequencies at first order in $\tilde{a}$. This was first shown by Kojima [19] using symmetry arguments for the axisymmetric case $m = 0$. Here we extend his argument to any value of m, for the generic set of equations (4) and (5). Let us start by noting that, at first order, Eqs. (4) and (5) are invariant under the simultaneous transformations

$$a_{\ell m} \to \mp a_{\ell -m}\,, \qquad p_{\ell m} \to \pm p_{\ell -m}\,, \tag{7a}$$

$$\tilde{a} \to -\tilde{a}\,, \qquad m \to -m\,, \tag{7b}$$

where $a_{\ell m}$ ($p_{\ell m}$) schematically denotes all of the axial (polar) perturbation variables with indices (ℓ, m). The invariance follows from the linearity of the terms in Eqs. (4) and (5) and from the fact that the $\mathcal{Q}_\ell$'s are *even* functions of m. The boundary conditions that define the characteristic modes of the BH are also invariant under the transformation above (cf. Eqs. (72) and (77) below). Therefore in the slow-rotation limit the eigenfrequencies can be expanded as

$$\omega = \omega_0 + m\,\omega_1 \tilde{a} + \omega_2 \tilde{a}^2 + \mathcal{O}(\tilde{a}^3)\,, \tag{8}$$

where ω_0 is the eigenfrequency of the nonrotating spacetime and ω_n is the n-th order correction (note that ω_1 and ω_2 are generically polynomials in m but, due to the above symmetry, ω_1 is an *even* polynomial). Crucially, only the terms ($\bar{\mathcal{P}}_\ell$, $\bar{\mathcal{A}}_\ell$) in Eqs. (4) and (5) can contribute to ω_1. Indeed, due to the factor $\tilde{a}$ in front of all terms ($\bar{\mathcal{P}}_\ell$, $\bar{\mathcal{A}}_\ell$, $\tilde{\mathcal{P}}_\ell$, $\tilde{\mathcal{A}}_\ell$) and to their linearity, at first order in $\tilde{a}$ we can simply take the zeroth order (in rotation) expansion of these terms. That is, to our level of approximation the terms ($\bar{\mathcal{P}}_\ell$, $\bar{\mathcal{A}}_\ell$, $\tilde{\mathcal{P}}_\ell$, $\tilde{\mathcal{A}}_\ell$) in Eqs. (4) and (5) only contain the perturbations of the *nonrotating*, spherically symmetric background. Since the latter do not explicitly depend on m, the m dependence in Eq. (8) can only arise from the terms ($\bar{\mathcal{P}}_\ell$, $\bar{\mathcal{A}}_\ell$) to zeroth order (recall that the $\mathcal{Q}_\ell$'s are even functions of m, so they do not contribute).

In the case of slowly rotating stars, this argument is reinforced by numerical simulations for the $m = 0$ axisymmetric modes [19] and in the general nonaxisymmetric case [63], which show that the coupling terms do not affect the first order corrections to the QNMs. In this work we shall verify that the same result holds also for massless vector (e.g. electromagnetic) modes and for Proca modes of a Kerr BH. If we are interested in the modes of the rotating background to $\mathcal{O}(\tilde{a})$ the coupling terms can therefore be neglected, and the eigenvalue problem can be written in the form

$$\mathcal{A}_\ell + \tilde{a} m \bar{\mathcal{A}}_\ell = 0\,, \tag{9}$$

$$\mathcal{P}_\ell + \tilde{a} m \bar{\mathcal{P}}_\ell = 0\,. \tag{10}$$

In these equations the polar and axial perturbations (as well as perturbations with different values of the harmonic indices) are decoupled from each other, and can be studied independently.

B. Eigenvalue spectrum to second order

For what concerns the calculation of the eigenfrequencies to second order in $\tilde{a}$, the equations above can be simplified as follows. To begin with, we remark that all of the coefficients in Eqs. (4) and (5) are *linear* combinations of axial or polar perturbation functions, $a_{\ell m}$, $p_{\ell m}$, respectively. These functions can be expanded in the rotation parameter as

$$\begin{aligned} a_{\ell m} &= a^{(0)}_{\ell m} + \tilde{a}\, a^{(1)}_{\ell m} + \tilde{a}^2 a^{(2)}_{\ell m} \\ p_{\ell m} &= p^{(0)}_{\ell m} + \tilde{a}\, p^{(1)}_{\ell m} + \tilde{a}^2 p^{(2)}_{\ell m}\,. \end{aligned} \tag{11}$$

The terms $\breve{\mathcal{A}}_{\ell\pm2}$ and $\breve{\mathcal{P}}_{\ell\pm2}$ are multiplied by factors $\tilde{a}^2$, so they only depend on the zeroth-order perturbation functions, $a^{(0)}_{\ell m}$, $p^{(0)}_{\ell m}$. The terms $\tilde{\mathcal{A}}_{\ell\pm1}$ and $\tilde{\mathcal{P}}_{\ell\pm1}$ are multiplied by factors $\tilde{a}$, so they only depend on zeroth- and first-order perturbation functions $a^{(0)}_{\ell m}$, $p^{(0)}_{\ell m}$, $a^{(1)}_{\ell m}$, $p^{(1)}_{\ell m}$.

Since in the nonrotating limit axial and polar perturbations are decoupled, a possible consistent set of solutions of the system (4)–(5) has $a^{(0)}_{\ell\pm2m} \equiv 0$; another consistent set of solutions of the same system has $p^{(0)}_{\ell\pm2m} \equiv 0$.

Such solutions, which we can call, following Refs. [29, 30], "axial-led" and "polar-led" perturbations respectively, can be found by solving the following subsets of the equations (4)–(5):

$$\mathcal{A}_\ell + \tilde{a} m \bar{\mathcal{A}}_\ell + \tilde{a}^2 \hat{\mathcal{A}}_\ell + \tilde{a}(\mathcal{Q}_\ell \tilde{\mathcal{P}}_{\ell-1} + \mathcal{Q}_{\ell+1}\tilde{\mathcal{P}}_{\ell+1}) = 0\,, \tag{12}$$

$$\mathcal{P}_{\ell+1} + \tilde{a} m \bar{\mathcal{P}}_{\ell+1} + \tilde{a}\mathcal{Q}_{\ell+1}\tilde{\mathcal{A}}_\ell = 0\,, \tag{13}$$

$$\mathcal{P}_{\ell-1} + \tilde{a} m \bar{\mathcal{P}}_{\ell-1} + \tilde{a}\mathcal{Q}_{\ell}\tilde{\mathcal{A}}_\ell = 0\,, \tag{14}$$

and

$$\mathcal{P}_\ell + \tilde{a} m \bar{\mathcal{P}}_\ell + \tilde{a}^2 \hat{\mathcal{P}}_\ell + \tilde{a}(\mathcal{Q}_\ell \tilde{\mathcal{A}}_{\ell-1} + \mathcal{Q}_{\ell+1}\tilde{\mathcal{A}}_{\ell+1}) = 0\,, \tag{15}$$

$$\mathcal{A}_{\ell+1} + \tilde{a} m \bar{\mathcal{A}}_{\ell+1} + \tilde{a}\mathcal{Q}_{\ell+1}\tilde{\mathcal{P}}_\ell = 0\,, \tag{16}$$

$$\mathcal{A}_{\ell-1} + \tilde{a} m \bar{\mathcal{A}}_{\ell-1} + \tilde{a}\mathcal{Q}_{\ell}\tilde{\mathcal{P}}_\ell = 0\,. \tag{17}$$

In the second and third equations of the two systems above we have dropped the $\tilde{\mathcal{A}}_{\ell\pm2}$ and $\tilde{\mathcal{P}}_{\ell\pm2}$ terms, because these only enter at zeroth order, and we have set $a^{(0)}_{\ell\pm2m} \equiv 0$ and $p^{(0)}_{\ell\pm2m} \equiv 0$.

Interestingly, within this perturbative scheme a notion of "conserved quantum number" ℓ is still meaningful, even though, for any given ℓ, rotation couples terms with opposite parity and different multipolar index. In the most relevant case from the point of view of superradiant instabilities, i.e. the case $\ell = m$, the last equations (14) and (17) are automatically satisfied, because $\mathcal{Q}_m = 0$ and perturbations with $\ell < m$ automatically vanish.

It is worth stressing that, even though in principle there may be modes which do not belong to the classes of "axial-led" or "polar-led" perturbations, all solutions belonging to one of these classes which fulfill the appropriate boundary conditions defining QNMs or bound states are also solutions of the full system (4)–(5) and belong to the eigenspectrum (up to second order in the rotation rate). This is particularly relevant since, as we shall show, these classes contain also superradiantly unstable modes.

In the case of massive scalar perturbations, as we show in the next section, the coupling to $\ell\pm2$ can be eliminated by defining a suitable linear combination of the eigenfunctions with different multipolar indices [cf. Eq. (37)], so that our procedure allows us to compute the entire BH spectrum up to second order. By a similar, suitable "rotation" in eigenfunction space it may be possible to recast Eqs. (4)–(5) in the forms (12)–(14) and (15)–(17), but we did not find a general proof of this conjecture. If the conjecture is correct, studying the "axial-led" and "polar-led" systems may be sufficient to describe the *entire* BH spectrum at second order in rotation.

To summarize, the eigenfrequencies (or at least a subset of the eigenfrequencies) of the general system (4)–(5) can be found, at first order in $\tilde{a}$, by solving the two decoupled sets (9) and (10) for axial and polar perturbations, respectively. At second order in $\tilde{a}$ we must solve either the set (12)–(14) or the set (15)–(17) for "axial-led" and "polar-led" modes, respectively. We conclude this section by noting that this procedure can be applied to any slowly rotating spacetime and to any kind of perturbation. For concreteness, in the next section we shall specialize the method to the case of massive scalar and vector perturbations of the Kerr metric.

III. MASSIVE SCALAR PERTURBATIONS OF SLOWLY ROTATING KERR BLACK HOLES

In order to illustrate how the slow-rotation expansion works, in this section we begin by working out the simplest case. We consider the massive Klein-Gordon equation for a scalar field perturbation ϕ around a rotating BH, and we work out the perturbation equations up to second order in rotation. The formalism applies to a generic stationary and axisymmetric background, but it is natural to focus on the case of interest in general relativity, i.e. the Kerr metric in Boyer-Lindquist coordinates:

$$ds^2_{\rm Kerr} = -\left(1 - \frac{2Mr}{\Sigma}\right)dt^2 + \frac{\Sigma}{\Delta}dr^2 - \frac{4rM^2}{\Sigma}\tilde{a}\sin^2\vartheta d\varphi dt$$
$$+\Sigma d\vartheta^2 + \left[(r^2 + M^2\tilde{a}^2)\sin^2\vartheta + \frac{2rM^3}{\Sigma}\tilde{a}^2\sin^4\vartheta\right]d\varphi^2\,, \tag{18}$$

where $\Sigma = r^2 + M^2\tilde{a}^2\cos^2\vartheta$, $\Delta = (r - r_+)(r - r_-)$ and $r_\pm = M(1 \pm \sqrt{1 - \tilde{a}^2})$. In what follows we shall expand the metric and all other quantities of interest to second order in $\tilde{a}$. At this order, the event horizon r_+, the Cauchy horizon r_- and the outer ergosphere r_{S^+} can be written in the form

$$r_+ = 2M\left(1 - \frac{\tilde{a}^2}{4}\right)\,, \quad r_- = \frac{M\tilde{a}^2}{2}\,,$$
$$r_{S^+} = 2M\left(1 - \cos^2\vartheta\frac{\tilde{a}^2}{4}\right)\,. \tag{19}$$

In particular, note that second-order corrections are necessary for the ergoregion to be located outside the event horizon.

The massive Klein-Gordon equation reads

$$\Box\phi = \mu^2\phi\,, \tag{20}$$

where $m_s = \mu\hbar$ is the mass of the scalar field. We decompose the field in spherical harmonics:

$$\phi = \sum_{\ell m}\frac{\Psi_\ell(r)}{\sqrt{r^2 + \tilde{a}^2M^2}}e^{-{\rm i}\,\omega t}Y^\ell(\vartheta,\varphi)\,, \tag{21}$$

and expand the square root above to second order in $\tilde{a}$. Schematically, we obtain the following equation:

$$A_\ell Y^\ell + D_\ell\cos^2\vartheta Y^\ell = 0\,, \tag{22}$$

where a sum over (ℓ, m) is implicit, and the explicit form of A_ℓ and D_ℓ is given in Appendix A 1. The crucial point

is that D_ℓ is proportional to $\tilde{a}^2$, so the second term in the equation above is zero to first order in rotation. If we consider a first-order expansion in rotation the scalar equation is already decoupled, and it can be cast in the form

$$\hat{\mathcal{D}}_2\Psi_\ell - \left[\frac{4mM^2\tilde{a}\omega}{r^3} + F\frac{2M}{r^3}\right]\Psi_\ell = 0\,, \tag{23}$$

where $F = 1-2M/r$, $dr/dr_* = F$ and we defined the operator [16]

$$\hat{\mathcal{D}}_2 = \frac{d^2}{dr_*^2} + \omega^2 - F\left[\frac{\ell(\ell+1)}{r^2} + \mu^2\right]. \tag{24}$$

Equation (23) coincides with Teukolsky's master equation [13] for spin $s=0$ perturbations expanded to first order in $\tilde{a}$. The coupling to perturbations with indices $\ell\pm1$ vanishes for a simple reason: Klein-Gordon perturbations are polar quantities, and at first order the Laporte-like selection rule implies that polar perturbations with index ℓ should couple to axial perturbations with $\ell\pm1$, but the latter are absent in the spin-0 case. At second order, perturbations with harmonic index ℓ are coupled to perturbations with the *same* parity and $\ell\pm2$, but this coupling does not contribute to the eigenfrequencies for the reasons discussed in the previous section. Therefore we must solve a single scalar equation for given values of ℓ and m, that we write schematically as

$$\mathcal{P}_\ell + \tilde{a}m\bar{\mathcal{P}}_\ell + \tilde{a}^2\hat{\mathcal{P}}_\ell = 0\,. \tag{25}$$

In order to confirm this general result, let us separate the angular part of Eq. (22). This can be achieved by using the identities [17]

$$\cos\vartheta Y^\ell = \mathcal{Q}_{\ell+1}Y^{\ell+1} + \mathcal{Q}_\ell Y^{\ell-1}\,, \tag{26}$$

$$\sin\vartheta\partial_\vartheta Y^\ell = \mathcal{Q}_{\ell+1}\ell Y^{\ell+1} - \mathcal{Q}_\ell(\ell+1)Y^{\ell-1}\,, \tag{27}$$

$$\cos^2\vartheta Y^\ell = \left(\mathcal{Q}_{\ell+1}^2 + \mathcal{Q}_\ell^2\right)Y^\ell + \mathcal{Q}_{\ell+1}\mathcal{Q}_{\ell+2}Y^{\ell+2} + \mathcal{Q}_\ell\mathcal{Q}_{\ell-1}Y^{\ell-2}\,, \tag{28}$$

$$\cos\vartheta\sin\vartheta\partial_\vartheta Y^\ell = \left(\ell\mathcal{Q}_{\ell+1}^2 - (\ell+1)\mathcal{Q}_\ell^2\right)Y^\ell + \mathcal{Q}_{\ell+1}\mathcal{Q}_{\ell+2}\ell Y^{\ell+2} - \mathcal{Q}_\ell\mathcal{Q}_{\ell-1}(\ell+1)Y^{\ell-2}\,, \tag{29}$$

as well as the orthogonality property of scalar spherical harmonics:

$$\int Y^\ell Y^{*\,\ell'}d\Omega = \delta^{\ell\ell'}\,. \tag{30}$$

The result reads, schematically,

$$A_\ell + (\mathcal{Q}_{\ell+1}^2 + \mathcal{Q}_\ell^2)D_\ell + \mathcal{Q}_{\ell-1}\mathcal{Q}_\ell D_{\ell-2} + \mathcal{Q}_{\ell+2}\mathcal{Q}_{\ell+1}D_{\ell+2} = 0\,. \tag{31}$$

By repeated use of the identity (26) we can separate the perturbation equations at *any order* in $\tilde{a}$. Indeed, because of the expansion in $\tilde{a}$, only combinations of the form $(\cos\vartheta)^n Y^\ell$ will appear. As we discuss in the next section this is also true for spin-1 or spin-2 perturbations, except that now the perturbation equations will contain combinations of vector and tensor spherical harmonics, and this introduces terms such as $(\sin\vartheta)^n\partial_\vartheta Y^\ell$, which can be decoupled in a similar fashion by repeated application of the identities listed above. This procedure is well known in quantum mechanics, and the coefficients $\mathcal{Q}_\ell$ are related to the usual Clebsch-Gordan coefficients.

Using the explicit form of the coefficients given in Appendix A 1, the field equations (31) schematically read

$$\frac{d^2\Psi_\ell}{dr_*^2} + V_\ell\Psi_\ell + \tilde{a}^2\Bigg[U_{\ell+2}\Psi_{\ell+2} + U_{\ell-2}\Psi_{\ell-2} + W_{\ell+2}\frac{d^2\Psi_{\ell+2}}{dr_*^2} + W_{\ell-2}\frac{d^2\Psi_{\ell-2}}{dr_*^2}\Bigg] = 0\,, \tag{32}$$

where we have defined the tortoise coordinate via $dr/dr_* \equiv f = \Delta/(r^2+a^2)$ (expanded at second order) and V, U and W are some potentials, whose explicit form is not needed here.

Note that the coupling to the $\ell\pm2$ terms is proportional to $\tilde{a}^2$. For a calculation accurate to second order in $\tilde{a}$ the terms in parenthesis can be evaluated at zeroth order, and therefore the functions $\Psi^{(0)}_{\ell\pm2}$ must be solutions of

$$\frac{d^2\Psi^{(0)}_{\ell\pm2}}{dr_*^2} + V^{(0)}_{\ell\pm2}\Psi^{(0)}_{\ell\pm2} = 0\,. \tag{33}$$

By substituting these relations in Eq. (32) we get

$$\frac{d^2\Psi_\ell}{dr_*^2} + V_\ell\Psi_\ell + \tilde{a}^2\left(U^{(0)}_{\ell+2} - V^{(0)}_{\ell+2}W^{(0)}_{\ell+2}\right)\Psi^{(0)}_{\ell+2} + \tilde{a}^2\left(U^{(0)}_{\ell-2} - V^{(0)}_{\ell-2}W^{(0)}_{\ell-2}\right)\Psi^{(0)}_{\ell-2} = 0\,. \tag{34}$$

Finally, making use of the expressions for V, U and W, the field equations can be reduced to

$$\frac{d^2\Psi_\ell}{dr_*^2} + V_\ell\Psi_\ell = \frac{\tilde{a}^2M^2(r-2M)\left(\mu^2-\omega^2\right)}{r^3} \times\left[\mathcal{Q}_{\ell+1}\mathcal{Q}_{\ell+2}\Psi^{(0)}_{\ell+2} + \mathcal{Q}_{\ell-1}\mathcal{Q}_\ell\Psi^{(0)}_{\ell-2}\right], \tag{35}$$

where the potential is given by

$$\begin{aligned} V_\ell =& \omega^2 - \left(1-\frac{2M}{r}\right)\left[\frac{\ell(\ell+1)}{r^2} + \frac{2M}{r^3} + \mu^2\right] \\ &- \frac{4\tilde{a}m\omega M^2}{r^3} \\ &+ \frac{\tilde{a}^2M^2}{r^6}\left[-24M^2 - 4Mr\left(\ell(\ell+1) - 3 + r^2\mu^2\right)\right. \\ &+ 2Mr^3\omega^2 + r^2\left(\ell(\ell+1) + m^2 + r^2(\mu^2-\omega^2) - 1\right) \\ &\left. - r^3(r-2M)(\mu^2-\omega^2)\left(\mathcal{Q}_\ell^2 + \mathcal{Q}_{\ell+1}^2\right)\right]. \end{aligned} \tag{36}$$

As we previously discussed, the couplings to terms with indices $\ell\pm2$ can be neglected in the calculation of the

modes. In the scalar case this can be shown explicitly as follows. If we define

$$Z_\ell = \psi_\ell - \tilde{a}^2 \left[c_{\ell+2}\psi_{\ell+2} - c_\ell \psi_{\ell-2} \right] , \tag{37}$$

where

$$c_\ell = \frac{M^2 \left(\mu^2 - \omega^2\right) \mathcal{Q}_{\ell-1}\mathcal{Q}_\ell}{2(2\ell-1)} , \tag{38}$$

then, at second order in rotation, Eq. (35) can be written as a single equation for Z_ℓ:

$$\frac{d^2 Z_\ell}{dr_*^2} + V_\ell Z_\ell = 0 , \tag{39}$$

which can be solved by standard methods. This equation coincides with Teukolsky's master equation [13] for spin $s = 0$ perturbations expanded at second order in $\tilde{a}$. This is a nontrivial consistency check for the slow-rotation expansion. In particular, the coefficients $\mathcal{Q}_\ell$ in Eq. (36) agree with an expansion of Teukolsky's spheroidal eigenvalues to second order in $\tilde{a}$ [64]. In fact, by extending our procedure to arbitrary order in $\tilde{a}$ we can reconstruct the Teukolsky scalar potential order by order. This can be viewed as an independent check of the standard procedure, which consists of expanding the angular equation to obtain the angular eigenfrequencies (see [64] and references therein).

In addition, as discussed in the previous section, the fact that neglecting the $\ell \pm 2$ couplings is equivalent to a field redefinition implies that the entire BH spectrum of (massive scalar) QNMs and bound states can be found by neglecting those couplings.

Finally, the near-horizon behavior of Eq. (39) reads

$$Z_\ell \sim e^{-\mathrm{i}\, k_H r_*} , \tag{40}$$

where $k_H = \omega - m\Omega_H$ and $\Omega_H \sim \tilde{a}/(4M) + \mathcal{O}(\tilde{a}^3)$. Note that, by virtue of the second order expansion, we get precisely $V_\ell \sim k_H^2$ close to the horizon.

The possibility to obtain a *single* equation for any given ℓ and m is a special feature of scalar perturbations. The underlying reason is that scalar perturbations have definite parity, so the mixing between perturbations of different parity cannot occur. As we show in the next section, this property does not necessarily hold for perturbations of higher spin.

IV. MASSIVE VECTOR PERTURBATIONS OF SLOWLY ROTATING KERR BLACK HOLES

The field equations of a massive vector field (also known as Proca's equation) read

$$\Pi^\nu \equiv \nabla_\sigma F^{\sigma\nu} - \mu^2 A^\nu = 0 , \tag{41}$$

where $F_{\mu\nu} = \partial_\mu A_\nu - \partial_\nu A_\mu$ and A_μ is the vector potential. Maxwell's equations are recovered when $\mu = m_v/\hbar = 0$, where m_v is the mass of the vector field. Note that, as a consequence of Eq. (41), the Lorenz condition $\nabla_\mu A^\mu = 0$ is automatically satisfied, i.e. in the massive case there is no gauge freedom and the field A_μ propagates $2s+1 = 3$ degrees of freedom [16].

In the $\mu = 0$ case, Teukolsky showed that the equations for spin-1 perturbations around a Kerr BH are separable [13], the angular part being described by spin-1 spheroidal harmonics. In the case of a massive field the separation does not appear to be possible, and one is left with a set of coupled partial differential equations. To avoid these difficulties we shall consider the slow-rotation limit of the Kerr metric and apply the approach described in Sec. II. The procedure is equivalent in spirit to that described for scalar perturbations, but it is more involved due to the spin-1 nature of the vector field.

A. Harmonic expansion of the Proca equation on a slowly rotating background

Following the notation of [63, 65] we set $x^\mu = (t, r, x^b)$ with $x^b = (\vartheta, \varphi)$. We also introduce the metric of the two-sphere $\gamma_{ab} = \mathrm{diag}(1, \sin^2\vartheta)$.

Any vector field can be decomposed in a set of vector spherical harmonics [65]

$$\begin{aligned} \mathbf{Y}^\ell_b &= \left(\partial_\vartheta Y^\ell, \partial_\varphi Y^\ell\right) , \\ \mathbf{S}^\ell_b &= \left(\frac{1}{\sin\vartheta}\partial_\varphi Y^\ell, -\sin\vartheta \partial_\vartheta Y^\ell\right) , \end{aligned} \tag{42}$$

where $Y^\ell(\vartheta, \varphi)$ are the scalar spherical harmonics. We expand the electromagnetic potential as follows [16]:

$$\delta A_\mu(t, r, \vartheta, \varphi) = \sum_{\ell,m} \begin{bmatrix} 0 \\ 0 \\ u^\ell_{(4)} \mathbf{S}^\ell_b/\Lambda \end{bmatrix} + \sum_{\ell,m} \begin{bmatrix} u^\ell_{(1)} Y^\ell/r \\ u^\ell_{(2)} Y^\ell/(rf) \\ u^\ell_{(3)} \mathbf{Y}^\ell_b/\Lambda \end{bmatrix} , \tag{43}$$

where $\Lambda = \ell(\ell+1)$. Because of their transformation properties under parity, the functions $u^\ell_{(i)}$ belong to the *polar* sector when $i = 1, 2, 3$, and to the *axial* sector when $i = 4$. In the nonrotating case the two sectors are decoupled [16]. The Proca equation (41), linearized in the perturbations $u^\ell_{(i)}$ $(i = 1, 2, 3, 4)$, can be written in the following form:

$$\begin{aligned} \delta\Pi_I \equiv{}& \left(A^{(I)}_\ell + \tilde{A}^{(I)}_\ell \cos\vartheta + D^{(I)}_\ell \cos^2\vartheta\right) Y^\ell \\ &+ \left(B^{(I)}_\ell + \tilde{B}^{(I)}_\ell \cos\vartheta\right) \sin\vartheta \partial_\vartheta Y^\ell = 0 , \end{aligned} \tag{44}$$

$$\begin{aligned} \delta\Pi_\vartheta \equiv{}& \left(\alpha_\ell + \rho_\ell \sin^2\vartheta\right) \partial_\vartheta Y^\ell - \mathrm{i}\, m\beta_\ell \frac{Y^\ell}{\sin\vartheta} \\ &+ \left(\eta_\ell + \sigma_\ell \cos\vartheta\right) \sin\vartheta Y^\ell = 0 , \end{aligned} \tag{45}$$

$$\begin{aligned} \frac{\delta\Pi_\varphi}{\sin\vartheta} \equiv{}& \left(\beta_\ell + \gamma_\ell \sin^2\vartheta\right) \partial_\vartheta Y^\ell + \mathrm{i}\, m\alpha_\ell \frac{Y^\ell}{\sin\vartheta} \\ &+ \left(\zeta_\ell + \lambda_\ell \cos\vartheta\right) \sin\vartheta Y^\ell = 0 , \end{aligned} \tag{46}$$

where a sum over (ℓ, m) is implicit and I denotes either the t component or the r component. The various radial

coefficients in the equations above are given in terms of the perturbation functions $u^{\ell}_{(i)}$ in Appendix A 2.

The perturbation equations (44)–(46) can be simplified by using the Lorenz identity $\nabla_\mu A^\mu = 0$. To second order in rotation, and for the background metric (18), this condition reads

$$\delta\Pi_L \equiv \left(A^{(2)}_\ell + \tilde{A}^{(2)}_\ell \cos\vartheta + D^{(2)}_\ell \cos^2\vartheta\right) Y^\ell + \left(B^{(2)}_\ell + \tilde{B}^{(2)}_\ell \cos\vartheta\right) \sin\vartheta \partial_\vartheta Y^\ell = 0\,, \quad (47)$$

where the various coefficients are again listed in Appendix A 2.

Each of the coefficients in Eqs. (44)–(47) is a linear combination of perturbation functions with either polar or axial parity (cf. Appendix A 2). Therefore we can divide them into two sets:

$$\begin{aligned} &\text{Polar:} \quad A^{(j)}_\ell\,, \quad \alpha_\ell\,, \quad \zeta_\ell\,, \quad \tilde{B}_\ell\,, \quad D_\ell\,, \quad \rho_\ell\,, \quad \sigma_\ell\,, \\ &\text{Axial:} \quad \tilde{A}^{(j)}_\ell\,, \quad B^{(j)}_\ell\,, \quad \beta_\ell\,, \quad \eta_\ell\,, \quad \lambda_\ell\,, \quad \gamma_\ell\,, \end{aligned}$$

where $j = 0, 1, 2$. In order to separate the angular variables in Eqs. (44)–(47) we compute the following integrals:

$$\int \delta\Pi_I Y^{*\,\ell} d\Omega\,, \quad (I = t, r, L)\,; \quad (48a)$$

$$\int \delta\Pi_a \mathbf{Y}^{*\,\ell}_b \gamma^{ab} d\Omega\,, \quad (a\,, b = \vartheta, \varphi)\,; \quad (48b)$$

$$\int \delta\Pi_a \mathbf{S}^{*\,\ell}_b \gamma^{ab} d\Omega\,, \quad (a\,, b = \vartheta, \varphi)\,. \quad (48c)$$

Using the orthogonality properties of scalar and vector harmonics, Eq. (30), the relations

$$\int \mathbf{Y}^{\ell}_b \mathbf{Y}^{*\,\ell'}_b \gamma^{ab} d\Omega = \int \mathbf{S}^{\ell}_b \mathbf{S}^{*\,\ell'}_b \gamma^{ab} d\Omega = \Lambda \delta^{\ell\ell'}\,,$$
$$\int \mathbf{Y}^{\ell}_b \mathbf{S}^{*\,\ell'}_b \gamma^{ab} d\Omega = 0\,, \quad (49)$$

as well as the identities (26)–(29), we find the following *radial* equations:

$$\begin{aligned} &A^{(I)}_\ell + \mathcal{Q}^2_{\ell+1}\left[D^{(I)}_\ell + \ell\tilde{B}^{(I)}_\ell\right] + \mathcal{Q}^2_\ell\left[D^{(I)}_\ell - (\ell+1)\tilde{B}^{(I)}_\ell\right] + \\ &\mathcal{Q}_\ell\left[\tilde{A}^{(I)}_{\ell-1} + (\ell-1)B^{(I)}_{\ell-1}\right] + \mathcal{Q}_{\ell+1}\left[\tilde{A}^{(I)}_{\ell+1} - (\ell+2)B^{(I)}_{\ell+1}\right] + \\ &\mathcal{Q}_{\ell-1}\mathcal{Q}_\ell\left[D^{(I)}_{\ell-2} + (\ell-2)\tilde{B}^{(I)}_{\ell-2}\right] \\ &+\mathcal{Q}_{\ell+2}\mathcal{Q}_{\ell+1}\left[D^{(I)}_{\ell+2} - (\ell+3)\tilde{B}^{(I)}_{\ell+2}\right] = 0\,, \end{aligned} \quad (50)$$

$$\begin{aligned} &\Lambda\alpha_\ell - \mathrm{i}\,m\zeta_\ell + \mathcal{Q}^2_{\ell+1}\ell\left[\ell\rho_\ell + \sigma_\ell\right] + \mathcal{Q}^2_\ell(\ell+1)\left[(\ell+1)\rho_\ell - \sigma_\ell\right] \\ &+\mathcal{Q}_\ell\left[-(\ell+1)\eta_{\ell-1} - \mathrm{i}\,m((\ell-1)\gamma_{\ell-1} + \lambda_{\ell-1})\right] \\ &+\mathcal{Q}_{\ell+1}\left[\ell\eta_{\ell+1} + \mathrm{i}\,m((\ell+2)\gamma_{\ell+1} - \lambda_{\ell+1})\right] \\ &-\mathcal{Q}_{\ell-1}\mathcal{Q}_\ell(\ell+1)\left[(\ell-2)\rho_{\ell-2} + \sigma_{\ell-2}\right] \\ &+\mathcal{Q}_{\ell+2}\mathcal{Q}_{\ell+1}\ell\left[-(\ell+3)\rho_{\ell+2} + \sigma_{\ell+2}\right] = 0\,, \end{aligned} \quad (51)$$

$$\begin{aligned} &\Lambda\beta_\ell + \mathrm{i}\,m\eta_\ell + \mathcal{Q}^2_{\ell+1}\ell\left[\ell\gamma_\ell + \lambda_\ell\right] + \mathcal{Q}^2_\ell(\ell+1)\left[(\ell+1)\gamma_\ell - \lambda_\ell\right] \\ &+\mathcal{Q}_\ell\left[-(\ell+1)\zeta_{\ell-1} + \mathrm{i}\,m((\ell-1)\rho_{\ell-1} + \sigma_{\ell-1})\right] \\ &+\mathcal{Q}_{\ell+1}\left[\ell\zeta_{\ell+1} - \mathrm{i}\,m((\ell+2)\rho_{\ell+1} - \sigma_{\ell+1})\right] \\ &-\mathcal{Q}_{\ell-1}\mathcal{Q}_\ell(\ell+1)\left[(\ell-2)\gamma_{\ell-2} + \lambda_{\ell-2}\right] \\ &+\mathcal{Q}_{\ell+2}\mathcal{Q}_{\ell+1}\ell\left[-(\ell+3)\gamma_{\ell+2} + \lambda_{\ell+2}\right] = 0\,. \end{aligned} \quad (52)$$

Note that Eqs. (50)–(52) have exactly the same structure as Eqs. (4)–(5).

B. Proca perturbation equations at first order

In order to make the equations more tractable, in this section we focus on the first-order corrections only. The second-order analysis is presented in Sec. IV C below. At first order, Eqs. (50)–(52) simplify to

$$\begin{aligned} &A^{(I)}_\ell + \mathcal{Q}_\ell\left[\tilde{A}^{(I)}_{\ell-1} + (\ell-1)B^{(I)}_{\ell-1}\right] \\ &+\mathcal{Q}_{\ell+1}\left[\tilde{A}^{(I)}_{\ell+1} - (\ell+2)B^{(I)}_{\ell+1}\right] = 0\,, \end{aligned} \quad (53)$$

$$\begin{aligned} &\Lambda\alpha_\ell - \mathrm{i}\,m\zeta_\ell \\ &-\mathcal{Q}_\ell(\ell+1)\eta_{\ell-1} + \mathcal{Q}_{\ell+1}\ell\eta_{\ell+1} = 0\,, \end{aligned} \quad (54)$$

$$\begin{aligned} &\Lambda\beta_\ell + \mathrm{i}\,m\eta_\ell \\ &-\mathcal{Q}_\ell(\ell+1)\zeta_{\ell-1} + \mathcal{Q}_{\ell+1}\ell\zeta_{\ell+1} = 0\,, \end{aligned} \quad (55)$$

where now the coefficients are linear in $\tilde{a}$.

To begin with, let us focus on the equations for monopole perturbations, $\ell = m = 0$. The longitudinal mode of a massive vector field (unlike the massless case) is dynamical. Since $m = 0$, the monopole only excites axisymmetric modes. In the nonrotating case these are described by a single equation belonging to the polar sector [55] (see also [16]); for $\ell = 0$, only the first two components $u^0_{(1)}$ and $u^0_{(2)}$ are defined. However, in the slowly rotating case these components are coupled to the $\ell = 1$ axial component $u^1_{(4)}$ through Eq. (53).

When $\ell = m = 0$, $\mathcal{Q}_0 = 0$ and Eq. (53) reduces to

$$A^{(I)}_0 + \mathcal{Q}_1\left[\tilde{A}^{(I)}_1 - 2B^{(I)}_1\right] = 0\,, \quad (56)$$

where $I = 0, 1, 2$. This is an extreme example of the "propensity rule" discussed in the general case: at first order the monopole is only coupled with axial perturbations with $\ell = 1$. Using the explicit form of the coefficients $A^{(I)}, \tilde{A}^{(I)}, B^{(I)}$ given in Appendix A 2 (truncated at first order), the equations above can be written as a single equation for $u^0_{(2)}$:

$$\left[\frac{d^2}{dr_*^2} + \omega^2 - F\left(\frac{2(r-3M)}{r^3} + \mu^2\right)\right] u^0_{(2)} = \frac{2\mathrm{i}\sqrt{3}\tilde{a}M^2\omega F}{r^3} u^1_{(4)}\,, \tag{57}$$

where at first order the tortoise coordinate r_* is the same as in the Schwarzschild case, and it is defined by $dr/dr_* = F$. The source term $u^1_{(4)}$ is the solution of Eq. (53) with $\ell = 1$. To first order in $\tilde{a}$ we can approximate $u^1_{(4)}$ (that is multiplied by $\tilde{a}$ in the source term) by its zeroth-order expansion in $\tilde{a}$, which is a solution of

$$\left\{\frac{d^2}{dr_*^2} + \omega^2 - F\left[\frac{2}{r^2} + \mu^2\right]\right\} u^1_{(4)} = 0\,. \tag{58}$$

Note that Eq. (58) is precisely the axial perturbation equation in the nonrotating case for $\ell = 1$ [16]. Eqs. (57) and (58) fully describe the dynamics of the polar $\ell = 0$ perturbations in the slow-rotation approximation. As we proved in Sec. II, the coupling on the right-hand side of Eq. (57) does not affect the QNMs to first order in rotation. In addition, since for the monopole $m = 0$, to this order the frequency is the same as in the Schwarzschild case, which is extensively discussed in Ref. [16].

Let us now turn to modes with $\ell > 0$. The equations for $\ell > 0$ at first order in $\tilde{a}$ are derived in Appendix B by using the Lorenz condition (B2) in order to eliminate $u^\ell_{(1)}$. The polar sector is fully described by the system

$$\begin{aligned}
&\hat{\mathcal{D}}_2 u^\ell_{(2)} - \frac{2F}{r^2}\left(1 - \frac{3M}{r}\right)\left[u^\ell_{(2)} - u^\ell_{(3)}\right] \\
&= \frac{2\tilde{a}M^2 m}{\Lambda r^5\omega}\left[\Lambda\left(2r^2\omega^2 + 3F^2\right)u^\ell_{(2)}\right. \\
&\left.+3F\left(r\Lambda F u'^\ell_{(2)} - \left(r^2\omega^2 + \Lambda F\right)u^\ell_{(3)}\right)\right] \\
&- \frac{6\mathrm{i}\,\tilde{a}M^2 F\omega}{\Lambda r^3}\left[(\ell+1)\mathcal{Q}_\ell u^{\ell-1}_{(4)} - \ell\mathcal{Q}_{\ell+1}u^{\ell+1}_{(4)}\right]\,, \qquad (59)\\
&\hat{\mathcal{D}}_2 u^\ell_{(3)} + \frac{2F\Lambda}{r^2}u^\ell_{(2)} = \\
&\frac{2\tilde{a}M^2 m}{r^5\omega}\left[2r^2\omega^2 u^\ell_{(3)} + 3rF^2 u'^\ell_{(3)} - 3\left(\Lambda + r^2\mu^2\right)F u^\ell_{(2)}\right]\,, \qquad (60)
\end{aligned}$$

where here and in the following a prime denotes derivation with respect to r and the operator $\hat{\mathcal{D}}_2$ is defined in Eq. (24). Note that while Eq. (60) only involves polar perturbations, in Eq. (59) we also have a coupling to $u^{\ell\pm1}_{(4)}$.

On the other hand, the axial sector leads to

$$\begin{aligned}
&\hat{\mathcal{D}}_2 u^\ell_{(4)} - \frac{4\tilde{a}M^2 m\omega}{r^3}u^\ell_{(4)} \\
&= -\frac{6\mathrm{i}\,\tilde{a}M^2 F}{r^5\omega}\left[(\ell+1)\mathcal{Q}_{\ell m}\psi^{\ell-1} - \ell\mathcal{Q}_{\ell+1m}\psi^{\ell+1}\right] \qquad (61)
\end{aligned}$$

(see Appendix B for details), where we have defined the polar function

$$\psi^\ell = \left(\Lambda + r^2\mu^2\right)u^\ell_{(2)} - (r-2M)u'^\ell_{(3)}\,. \tag{62}$$

Note that this term is similar to Eq.(25) in Ref. [16]. As expected, the axial perturbation $u^\ell_{(4)}$ is coupled to the polar functions with $\ell \pm 1$. Equations (59), (60) and (61) describe the massive vector perturbations of a Kerr BH to first order in $\tilde{a}$ for $\ell > 0$. These equations reduce to those in Ref. [16] when $\tilde{a} = 0$.

Since the right-hand side of Eq. (61) is proportional to $\tilde{a}$, in our perturbative framework we can *first* solve for $u^{\ell\pm1}_{(2)}$ and $u^{\ell\pm1}_{(3)}$ to zeroth order in the rotation rate, and then use these solutions as a source term in Eq. (61). As we proved in Sec. II, the coupling on the right-hand side of Eq. (61) does not affect the QNMs to first order in rotation. In Sec. VI we shall verify this property numerically. Therefore, for the purpose of computing eigenfrequencies to first order in $\tilde{a}$ we can simply consider the following polar equations:

$$\begin{aligned}
&\hat{\mathcal{D}}_2 u^\ell_{(2)} - \frac{2F}{r^2}\left(1 - \frac{3M}{r}\right)\left[u^\ell_{(2)} - u^\ell_{(3)}\right] \\
&= \frac{2\tilde{a}M^2 m}{\Lambda r^5\omega}\left[\Lambda\left(2r^2\omega^2 + 3F^2\right)u^\ell_{(2)}\right. \\
&\left.+3F\left(r\Lambda F u'^\ell_{(2)} - \left(r^2\omega^2 + \Lambda F\right)u^\ell_{(3)}\right)\right]\,, \qquad (63)\\
&\hat{\mathcal{D}}_2 u^\ell_{(3)} + \frac{2F\Lambda}{r^2}u^\ell_{(2)} = \\
&\frac{2\tilde{a}M^2 m}{r^5\omega}\left[2r^2\omega^2 u^\ell_{(3)} + 3rF^2 u'^\ell_{(3)} - 3\left(\Lambda + r^2\mu^2\right)F u^\ell_{(2)}\right]\,, \qquad (64)
\end{aligned}$$

as well as the decoupled axial equation

$$\hat{\mathcal{D}}_2 u^\ell_{(4)} - \frac{4\tilde{a}M^2 m\omega}{r^3}u^\ell_{(4)} = 0\,. \tag{65}$$

Within our perturbative scheme, any eigenfrequency of Eq. (65) is also a solution of the coupled Eq. (61) as long as $u^{\ell\pm1}_{(2)} = u^{\ell\pm1}_{(3)} = 0$, which is a trivial solution of Eqs. (59) and (60) for $\ell \pm 1$ at zeroth order. Furthermore, consistently with our argument in Sec. II, we have checked that there are no other modes to order $\mathcal{O}(\tilde{a})$ (cf. Sec. VI).

Note the similarity between Eq. (65), describing axial Proca modes, and Eq. (23) for massive scalar perturbations. Indeed, one can show that the generalization of Eq. (65) to the background metric (2) (i.e. without specializing to the slowly rotating Kerr metric) can be

written in a form that includes also massive *scalar* perturbations. This "master equation" reads

$$FB\Psi_\ell'' + \frac{1}{2}\left[B'F + F'B\right]\Psi_\ell' + \left[\omega^2 - \frac{2m\varpi(r)\omega}{r^2} - F\left(\frac{\Lambda}{r^2} + \mu^2 + (1-s^2)\left\{\frac{B'}{2r} + \frac{BF'}{2rF}\right\}\right)\right]\Psi_\ell = 0\,, \tag{66}$$

and it can be simplified by introducing a generalized tortoise coordinate $y(r)$ such that $dr/dy = \sqrt{FB}$. In the equation above s is the spin of the perturbation ($s = 0$ for scalar perturbations and $s = \pm 1$ for vector perturbations with axial parity). In the nonrotating case Eq. (66) is exact; it also includes gravitational perturbations of a Schwarzschild BH if $s = \pm 2$ and $F = B = 1 - 2M/r$. In the slowly rotating case Eq. (66) is a complete description of massive scalar perturbations for $s = 0$, whereas for $s = \pm 1$ it describes the axial sector without the $\ell \to \ell \pm 1$ couplings, i.e. it is a generalization of Eq. (65).

C. Proca perturbation equations at second order

In this section we briefly present the derivation of the Proca eigenvalue problem to second order in $\tilde{a}$.

By using the Lorenz condition to eliminate the spurious $u^\ell_{(1)}$ mode, Eqs. (50)–(52) can be written as

$$\mathcal{D}_{\mathbf{A}}{\boldsymbol{\Psi}_{\mathbf{A}}}^\ell + \mathbf{V}_{\mathbf{A}}{\boldsymbol{\Psi}_{\mathbf{A}}}^\ell = 0\,, \tag{67}$$

$$\mathcal{D}_{\mathbf{P}}{\boldsymbol{\Psi}_{\mathbf{P}}}^\ell + \mathbf{V}_{\mathbf{P}}{\boldsymbol{\Psi}_{\mathbf{P}}}^\ell = 0\,, \tag{68}$$

where $\mathcal{D}_{\mathbf{A},\mathbf{P}}$ are second order differential operators, $\mathbf{V}_{\mathbf{A},\mathbf{P}}$ are matrices, ${\boldsymbol{\Psi}_{\mathbf{A}}}^\ell = (u^\ell_{(4)}, u^{\ell\pm1}_{(2)}, u^{\ell\pm1}_{(3)}, u^{\ell\pm2}_{(4)})$ and ${\boldsymbol{\Psi}_{\mathbf{P}}}^\ell = (u^\ell_{(2)}, u^\ell_{(3)}, u^{\ell\pm1}_{(4)}, u^{\ell\pm2}_{(2)}, u^{\ell\pm2}_{(3)})$. The explicit form of the equations above is quite lengthy; therefore we do not show it in this article, but we make it available online [61]. It can be obtained using the procedure explained above and the coefficients listed in Appendix A 2. The function $u^\ell_{(1)}$ can be obtained from the Lorenz condition once the three dynamical degrees of freedom are known. Note that Eqs. (70)-(71) are particular cases of Eqs. (12)-(14) and Eqs. (15)-(17), respectively.

If we are interested in the eigenfrequencies up to second order in $\tilde{a}$ we can drop the couplings to $\ell \pm 2$ perturbations, for reasons discussed in Sec. II. Therefore, a consistent subset of Eqs. (50)–(52) reads

$$\begin{aligned}
0 =\ & A^{(i)}_\ell + \mathcal{Q}^2_{\ell+1}\left[D^{(i)}_\ell + \ell\tilde{B}^{(i)}_\ell\right] \\
& + \mathcal{Q}^2_\ell\left[D^{(i)}_\ell - (\ell+1)\tilde{B}^{(i)}_\ell\right] + \mathcal{Q}_\ell\left[\tilde{A}^{(i)}_{\ell-1} + (\ell-1)B^{(i)}_{\ell-1}\right] \\
& + \mathcal{Q}_{\ell+1}\left[\tilde{A}^{(i)}_{\ell+1} - (\ell+2)B^{(i)}_{\ell+1}\right]\,, \\
0 =\ & \Lambda\alpha_\ell - \mathrm{i}\,m\zeta_\ell + \mathcal{Q}^2_{\ell+1}\ell\left[\ell\rho_\ell + \sigma_\ell\right] \\
& + \mathcal{Q}^2_\ell(\ell+1)\left[(\ell+1)\rho_\ell + \sigma_\ell\right] \\
& + \mathcal{Q}_\ell\left[-(\ell+1)\eta_{\ell-1} - \mathrm{i}\,m((\ell-1)\gamma_{\ell-1} + \lambda_{\ell-1})\right] \\
& + \mathcal{Q}_{\ell+1}\left[\ell\eta_{\ell+1} + \mathrm{i}\,m((\ell+2)\gamma_{\ell+1} - \lambda_{\ell+1})\right]\,, \\
0 =\ & \Lambda\beta_\ell + \mathrm{i}\,m\eta_\ell + \mathcal{Q}^2_{\ell+1}\ell\left[\ell\gamma_\ell + \lambda_\ell\right] \\
& + \mathcal{Q}^2_\ell(\ell+1)\left[(\ell+1)\gamma_\ell + \lambda_\ell\right] \\
& + \mathcal{Q}_\ell\left[-(\ell+1)\zeta_{\ell-1} + \mathrm{i}\,m((\ell-1)\rho_{\ell-1} + \sigma_{\ell-1})\right] \\
& + \mathcal{Q}_{\ell+1}\left[\ell\zeta_{\ell+1} - \mathrm{i}\,m((\ell+2)\rho_{\ell+1} - \sigma_{\ell+1})\right]\,.
\end{aligned} \tag{69}$$

As in the scalar case, the second-order coefficients generally contain second derivatives of the perturbation functions, i.e. $u''^\ell_{(i)}$, $u''^{\ell\pm1}_{(i)}$ and $u''^{\ell\pm2}_{(i)}$. Since the coefficients are already of second order, we can use the perturbation equations *in the nonrotating limit* in order to eliminate these second derivatives. After some manipulation we get the final two sets of equations, that can be schematically written as

$$\mathcal{D}'_{\mathbf{A}}{\boldsymbol{\Upsilon}_{\mathbf{A}}}^\ell + \mathbf{V}'_{\mathbf{A}}{\boldsymbol{\Upsilon}_{\mathbf{A}}}^\ell = 0\,, \tag{70}$$

$$\mathcal{D}'_{\mathbf{P}}{\boldsymbol{\Upsilon}_{\mathbf{P}}}^\ell + \mathbf{V}'_{\mathbf{P}}{\boldsymbol{\Upsilon}_{\mathbf{P}}}^\ell = 0\,, \tag{71}$$

where $\mathcal{D}'_{\mathbf{A},\mathbf{P}}$ are second order differential operators, ${\boldsymbol{\Upsilon}_{\mathbf{A}}}^\ell = (u^\ell_{(4)}, u^{\ell\pm1}_{(2)}, u^{\ell\pm1}_{(3)})$, ${\boldsymbol{\Upsilon}_{\mathbf{P}}}^\ell = (u^\ell_{(2)}, u^\ell_{(3)}, u^{\ell\pm1}_{(4)})$, and $\mathbf{V}'_{\mathbf{A},\mathbf{P}}$ are matrices.

We remark that for a given value of ℓ and m, $\boldsymbol{\Upsilon}_{\mathbf{A}}$ and $\boldsymbol{\Upsilon}_{\mathbf{P}}$ are five- and four-dimensional vectors, respectively, while $\boldsymbol{\Psi}_{\mathbf{A}}$ and $\boldsymbol{\Psi}_{\mathbf{P}}$ in Eqs. (67) and (68) are seven- and eight-dimensional vectors, respectively. This is a very convenient simplification, because large systems of equations are computationally more demanding. Furthermore the couplings to perturbations with index $\ell - 1$ vanish if $\ell = m$, because as usual the factors $\mathcal{Q}_m = 0$, and in this case we are left with two subsystems of dimension three.

V. THE EIGENVALUE PROBLEM FOR QUASINORMAL MODES AND BOUND STATES

One of the key advantages of the slow-rotation approximation is that the perturbation equations can be solved using well-known numerical approaches. The integration proceeds exactly in the same way as in the nonrotating case. For example, for Proca perturbations of a slowly rotating Kerr BH we can compute the characteristic modes by following a procedure similar to the Schwarzschild case discussed in Ref. [16], as follows.

The perturbation equations (70)–(71), together with appropriate boundary conditions at the horizon and at infinity, form an eigenvalue problem for the frequency

spectrum. In the near-horizon limit, $\mathcal{D}_{\mathbf{A},\mathbf{P}} \to d^2/dr_*^2$ and $\mathbf{V}_{\mathbf{A},\mathbf{P}} \to (\omega - m\Omega_H)^2$, so that at the horizon we impose purely ingoing-wave boundary conditions:

$$u^\ell_{(i)} \sim u^\ell_{(i)H} e^{-\mathrm{i}\, k_H r_*}\,, \tag{72}$$

where $u^\ell_{(i)H}$ is a constant and

$$k_H = \omega - m\Omega_H = \omega - \frac{m\tilde{a}}{4M} + \mathcal{O}(\tilde{a}^3)\,. \tag{73}$$

We have introduced the horizon angular frequency $\Omega_H = a/(2Mr_+)$ and expanded it to second order.

In the massless case, due to the boundary condition (72), superradiant scattering for scalar, electromagnetic and gravitational perturbations is possible when $\omega_R < m\Omega_H$ [66], i.e. (to second order in rotation) when

$$\tilde{a} > \frac{4M\omega_R}{m}\,, \tag{74}$$

where ω_R is the real part of the mode frequency, i.e. $\omega = \omega_R + \mathrm{i}\,\omega_I$. Superradiance is possible because the energy flux at the horizon

$$\dot{E}_{r_+} \equiv \lim_{r\to r_+} \int d\vartheta d\varphi \sqrt{-g} T^r_t \tag{75}$$

is *negative* when $k_H < 0$. In the equation above $T_{\mu\nu}$ is the stress-energy tensor of the perturbation. The same argument can be applied to massive scalar perturbations.

The case of massive vector perturbations is more involved. For purely axial perturbations close to the horizon, by using Eq. (75) and the stress-energy tensor of a Proca field we get $\dot{E}_{r_+} = \sum_{\ell m} \dot{E}^\ell_{r_+}$ with

$$\dot{E}^\ell_{r_+} = \frac{\omega k_H}{4\ell(\ell+1)M^6} |u^\ell_{(4)H}|^2 + \mathcal{O}(\tilde{a}^3)\,, \tag{76}$$

which shows that the energy flux across the horizon is negative when $k_H < 0$. The general case involves terms proportional to each component $u^\ell_{(i)H}$, as well as terms proportional to μ^2.

As we discuss in Sec. VI below, our results turn out to be very accurate for moderate values of $\tilde{a}$ and they are reliable even in the superradiant regime, defined by Eq. (74), as long as $\omega_R M \ll 1$. Superradiant scattering leads to instabilities for massive scalar perturbations [35, 60]. In the Proca case, the numerical results discussed in Sec. VI below show that, when the superradiant condition (74) is met, the imaginary part of the modes crosses zero. Thus our numerical data show hard evidence, for the first time, that massive vector fields trigger (as expected) a superradiant instability.

The asymptotic behavior of the solution at infinity reads

$$u^\ell_{(i)} \sim B_{(i)} e^{-k_\infty r} r^{-\frac{M(\mu^2-2\omega^2)}{k_\infty}} + C_{(i)} e^{k_\infty r} r^{\frac{M(\mu^2-2\omega^2)}{k_\infty}}\,, \tag{77}$$

where $k_\infty = \sqrt{\mu^2 - \omega^2}$, so that $\mathrm{Re}[\mathrm{k}_\infty] > 0$. The boundary conditions $B_{(i)} = 0$ yield purely outgoing waves at infinity, i.e. QNMs [4]. If instead we impose $C_{(i)} = 0$ we get states that are spatially localized within the vicinity of the BH and decay exponentially at spatial infinity, i.e. bound states (see e.g. [16, 35]). Stable QNMs are more challenging to compute than bound states. In the former case the boundary conditions above imply that purely outgoing waves blow up as $r_* \to \infty$, whereas purely ingoing waves are exponentially suppressed at infinity. For bound states, direct integration of the equations combined with a shooting method is sufficient, but QNMs are more efficiently computed by other means, for example via continued fraction methods [4].

A. On the superradiant regime and the second order expansion

Here we comment on some important features that would be missed in a first order treatment. First, at second order the structure of the background metric is remarkably different, because all metric coefficients acquire $\mathcal{O}(\tilde{a}^2)$ corrections. This affects the location of the event horizon, of the ergosphere and of the inner Cauchy horizon [cf. Eq. (19)]. Second-order corrections are known to approximate the Kerr solution much better than a first-order expansion (see e.g. [67]).

From a dynamical point of view, axisymmetric modes acquire second-order corrections that break the $m = 0$ degeneracy of the first-order case. Most importantly, at second order the superradiant regime of vector and scalar fields can be described within our perturbative approach in a *self-consistent* way. The superradiant condition (74) may look like a first-order effect. However, at the onset of superradiance $\omega M \sim \tilde{a}$ (at least in the most relevant cases, i.e. when m is of order unity). In this case, terms like ω^2 in the field equations (which are crucial, in particular in the study of the mode spectrum) are of the same order of magnitude as second order quantities.

The field equations are of second differential order, so the linearized field equations (at *first* order in $\tilde{a}$) contain at most terms of order

$$\omega M\,, \quad (\omega M)^2\,, \quad \tilde{a}\,, \quad \tilde{a}\omega M\,. \tag{78}$$

In principle, terms of order $\tilde{a}(\omega M)^2$ would also be allowed, but those do not appear in the linearized Proca equations (50)–(52). In the massless case this is consistent with a first-order expansion of the Teukolsky equation, which does not contain any $\tilde{a}(\omega M)^2$ term for scalar, vector and tensor perturbations.

Thus, if $\omega M \sim \tilde{a}$ the second and fourth terms listed above would be as large as second-order terms in $\tilde{a}$, which are neglected in a first-order expansion. In a second-order expansion, instead, one also keeps terms proportional to $\tilde{a}^2$. This would be enough to consistently describe the superradiant regime up to first order in $\tilde{a}$, i.e. up to terms

$\sim \tilde{a}\omega$ and $\sim \omega^2$. For a related discussion in the case of neutron star r-modes, we refer the reader to Ref. [68].

B. Continued fraction method for quasinormal modes and bound states

From a conceptual point of view, numerical calculations in the slow-rotation approximation are not more complicated than in the nonrotating case. For example, in order to apply the continued fraction method we can write down a recurrence relation similar to Eqs. (31) and (32) of Ref. [16], starting from Eqs. (59), (60) and (65), by imposing the ansatz

$$u^{\ell}_{(i)} = (r-r_+)^{-2ik_H} r^{\nu} e^{-qr} \sum_n a^{(i)}_n (r-r_+)^n \,, \qquad (79)$$

where $\nu = -q + \omega^2/q + 2ik_H$ and $q = \pm k_\infty$ for bound states and for QNMs, respectively. For the axial equation this ansatz leads to a three-term recurrence relation of the form

$$\alpha_0 a^{(4)}_1 + \beta_0 a^{(4)}_0 = 0 \,,$$
$$\alpha_n a^{(4)}_{n+1} + \beta_n a^{(4)}_n + \gamma_n a^{(4)}_{n-1} = 0 \,, \quad n>0 \,,$$

whose coefficients (to first order in $\tilde{a}$, and setting $M=1$ in these equations only) read

$$\alpha_n = -4(1+n)q^2(1+n-4\mathrm{i}\,\omega) - 4\mathrm{i}\,\tilde{a}m(1+n)q^2 \qquad (80)$$

$$\begin{aligned}\beta_n = {} & 4q\left(q(1+\ell(\ell+1)+2n^2+q(3+4q)\right. \\ & \left. +n(2+6q)-s^2\right) - 4\mathrm{i}\,q(1+2n+3q)\omega \\ & -(1+2n+12q)\omega^2 + 4\mathrm{i}\,\omega^3) \\ & +4\mathrm{i}\,\tilde{a}mq\left(q+2nq+3q^2-2\mathrm{i}\,q\omega-\omega^2\right) \,, \end{aligned} \qquad (81)$$

$$\begin{aligned}\gamma_n = {} & -4\left[(q(n+q)-2\mathrm{i}\,q\omega-\omega^2)^2 - s^2q^2\right] \\ & -4\mathrm{i}\,\tilde{a}mq\left(q(n+q)-2\mathrm{i}\,q\omega-\omega^2\right) \,, \end{aligned} \qquad (82)$$

for $s=\pm 1$. If we set $s=0$, the equations above are also valid for massive *scalar* perturbations of a Kerr BH in the slowly rotating limit because, as we have shown above, there exists a single master equation describing both massive scalar and axial vector modes [cf. Eq. (66)]. We have investigated the massive scalar case to test the robustness of our results, because in this case the perturbation equations on a generic Kerr background are separable [60] and the eigenvalues can be computed by a direct solution of the Teukolsky equation [4, 35].

In the slowly rotating case the polar sector leads to a six-term, matrix-valued [16] recurrence relation

$$\begin{aligned}
&\boldsymbol{\alpha}_0\mathbf{U}_1 + \boldsymbol{\beta}_0\mathbf{U}_0 = 0 \,, \\
&\boldsymbol{\alpha}_1\mathbf{U}_2 + \boldsymbol{\beta}_1\mathbf{U}_1 + \boldsymbol{\gamma}_1\mathbf{U}_0 = 0 \,, && n>0 \,, \\
&\boldsymbol{\alpha}_2\mathbf{U}_3 + \boldsymbol{\beta}_2\mathbf{U}_2 + \boldsymbol{\gamma}_2\mathbf{U}_1 + \boldsymbol{\delta}_2\mathbf{U}_0 = 0 \,, && n>1 \,, \\
&\boldsymbol{\alpha}_3\mathbf{U}_4 + \boldsymbol{\beta}_3\mathbf{U}_3 + \boldsymbol{\gamma}_3\mathbf{U}_2 + \boldsymbol{\delta}_3\mathbf{U}_1 + \boldsymbol{\rho}_3\mathbf{U}_0 = 0 \,, && n>2 \,, \\
&\boldsymbol{\alpha}_n\mathbf{U}_{n+1} + \boldsymbol{\beta}_n\mathbf{U}_n + \boldsymbol{\gamma}_n\mathbf{U}_{n-1} + \boldsymbol{\delta}_n\mathbf{U}_{n-2} \\
&+\boldsymbol{\rho}_n\mathbf{U}_{n-3} + \boldsymbol{\sigma}_n\mathbf{U}_{n-4} = 0 \,, && n>3 \,,
\end{aligned}$$

where $\mathbf{U}_n = (a^{(2)}_n, a^{(3)}_n)$ is a two-dimensional vectorial coefficient and $\boldsymbol{\alpha}_n$, $\boldsymbol{\beta}_n$, $\boldsymbol{\gamma}_n$, $\boldsymbol{\delta}_n$, $\boldsymbol{\rho}_n$ and $\boldsymbol{\sigma}_n$ are 2×2 matrices, whose explicit form we do not present here for brevity but it is available online [61]. By using a matrix-valued Gaussian elimination [4, 69, 70] the system above can be reduced to a three-term matrix-valued recurrence relation, which can be solved with the method discussed in Ref. [16].

The continued fraction method works very well for both QNMs and bound-state modes. We computed QNMs and checked that they yield the correct limit in the massless case (see Sec. VI B below), but in the following we will focus mainly on bound states, that can become unstable in the superradiant regime.

C. Direct integration and Breit-Wigner resonance method for bound states

To compute bound state frequencies it is possible to use either a direct integration method or the Breit-Wigner resonance method. We start with a series expansion of the solution close to the horizon:

$$u^{\ell}_{(i)} \sim e^{-\mathrm{i}\,k_H r_*} \sum_n b^{(i)}_n (r-r_+)^n \,, \qquad (83)$$

where r_+ is expanded to second order and the coefficients $b^{(i)}_n$ ($n>0$) can be computed in terms of $b^{(i)}_0$ by solving the near-horizon equations order by order. In the direct integration method, the field equations are integrated outwards up to infinity, where the condition $C_{(i)}=0$ in Eq. (77) is imposed (see Ref. [16] for details).

The Breit-Wigner resonance method, also known as the standing-wave approach [63, 71–73], is well suited to computing QNMs and bound states of the system of equations (59)–(61) in the case of slowly damped modes, i.e. those with $\omega_I \ll \omega_R$. In this case the eigenvalue problem can be solved by looking for minima of a real-valued function of a real variable [72]. We briefly explain the procedure below, where we extend it to deal with a system of coupled equations. For clarity we only consider first-order corrections, but our argument applies also to the second-order case described by Eqs. (70)–(71) and, in principle, to any order.

Since $\ell = 0, 1, 2, ..$, the full system (59), (60) and (61) formally contains an *infinite* number of equations. In practice, we can truncate it at some given value of ℓ, compute the modes as explained below, and finally check convergence by increasing the truncation order. Let us suppose we truncate the axial sector at $\ell = L$ and the polar sector at $\ell = L+1$, i.e. for a given m we assume

$$u^{\ell}_{(4)} \equiv 0 \,, \qquad u^{\ell+1}_{(j)} \equiv 0 \qquad \text{when} \qquad \ell \geq L \,, \qquad (84)$$

with $j=1,2,3$ denoting the polar perturbations. All perturbations vanish identically for $\ell < |m|$.

When $m=0$, the truncation above reduces the system to $N = 3L$ coupled second-order ODEs for $L-1$

axial functions and $2L+1$ polar functions, including the monopole, described by Eq. (57). When $|m|>0$ the truncated system contains $N=3L-3|m|+2$ second-order ODEs (for $L-|m|$ axial functions and $2L-2|m|+2$ polar functions). In all cases we are left with a system of N second-order ODEs for N perturbation functions, which we collectively denote by $y_{(p)}$ $(p=1,...,N)$.

At the horizon each function is described by ingoing and outgoing waves. We impose a purely ingoing wave boundary condition analogous to Eq. (83),

$$y_{(p)} \sim e^{-\mathrm{i}\, k_H r_*} \sum_n c_n^{(p)} (r-r_+)^n \,, \tag{85}$$

where again the coefficients $c_n^{(p)}$ $(n>0)$ can be computed in terms of $c_0^{(p)}$. A family of solutions at infinity is then characterized by N parameters, corresponding to the N-dimensional vector of the near-horizon coefficients, $\mathbf{c_0}=\{c_0^{(p)}\}$. At infinity we look for exponentially decaying solutions, which correspond to bound, slowly damped modes. The spectrum of these modes can be obtained as follows. We first choose a suitable orthogonal basis for the N-dimensional space of the initial coefficients $c_0^{(p)}$ (see also Ref. [16]). We perform N integrations from the horizon to infinity and construct the $N\times N$ matrix

$$\mathbf{S}_m(\omega) = \lim_{r\to\infty} \begin{pmatrix} y_{(1)}^{(1)} & y_{(1)}^{(2)} & ... & y_{(1)}^{(N)} \\ y_{(2)}^{(1)} & y_{(2)}^{(2)} & ... & ... \\ ... & ... & ... & ... \\ ... & ... & ... & ... \\ y_{(N)}^{(1)} & ... & ... & y_{(N)}^{(N)} \end{pmatrix} , \tag{86}$$

where the superscripts denote a particular vector of the basis, i.e. $y_{(p)}^{(1)}$ corresponds to $\mathbf{c_0}=\{1,0,0,...,0\}$, $y_{(p)}^{(2)}$ corresponds to $\mathbf{c_0}=\{0,1,0,...,0\}$ and $y_{(p)}^{(N)}$ corresponds to $\mathbf{c_0}=\{0,0,0,...,1\}$. Finally, the bound-state frequency $\omega_0=\omega_R+\mathrm{i}\,\omega_I$ is obtained by imposing

$$\det \mathbf{S}_m(\omega_0)=0\,. \tag{87}$$

So far we have not imposed the Breit-Wigner assumption $\omega_I \ll \omega_R$. In fact, the procedure discussed above can be used to perform a general direct integration in the case of coupled systems.

By expanding Eq. (87) about ω_R and assuming $\omega_I \ll \omega_R$ we get [63]

$$\det \mathbf{S}_m(\omega_0) \simeq \det \mathbf{S}_m(\omega_R) + \mathrm{i}\,\omega_I \left.\frac{d\left[\det \mathbf{S}_m(\omega)\right]}{d\omega}\right|_{\omega_R} = 0\,, \tag{88}$$

which gives a relation between $d\left[\det \mathbf{S}_m(\omega)\right]/d\omega$ and $\det \mathbf{S}_m$ at $\omega=\omega_R$. We consider the function $\det \mathbf{S}_m$ restricted to real values of ω. A Taylor expansion for (real) ω close to ω_R yields (using the relation above):

$$\det \mathbf{S}_m(\omega) \simeq \det \mathbf{S}_m(\omega_R)\left[1-\frac{\omega-\omega_R}{\mathrm{i}\,\omega_I}\right] \propto \omega-\omega_R-\mathrm{i}\,\omega_I\,. \tag{89}$$

Therefore, on the real–ω axis, close to the real part of the mode,

$$\left|\det \mathbf{S}_m\left(\omega\right)\right|^2 \propto \left(\omega-\omega_R\right)^2+\omega_I^2\,. \tag{90}$$

To summarize, to find the slowly damped modes it is sufficient to integrate the truncated system N times for real values of the frequency ω, construct the matrix $\mathbf{S}_m\left(\omega\right)$ and find the minima of the function $|\det \mathbf{S}_m|^2$, which represent the real part of the modes. Then the imaginary part (in modulus) of the mode can be extracted through a quadratic fit, as in Eq. (90). We note that the same method can be straightforwardly extended to compute the slowly damped modes of the general systems (12)–(14) and (15)–(17).

	$M\omega_R$	$M\omega_I$
No coupling, $\ell=1$ (DI)	0.099484532	$1.1\cdot 10^{-7}$
Full system, $L=1,2,3,4$ (BW)	0.099484563	$1.1\cdot 10^{-7}$
No coupling, $\ell=1$ (DI)	0.09987320753	$4\cdot 10^{-11}$
Full system, $L=2,3,4$ (BW)	0.09987183250	$5\cdot 10^{-11}$

TABLE I. Examples of polar (top rows) and axial (bottom rows) bound-state modes for $m=1$, $M\mu=0.1$ and $\tilde{a}=0.1$ computed at first order. Modes were computed via direct integration (DI) of the system (59)–(60) *without* couplings $\ell\to\ell\pm1$, as well as with the Breit-Wigner (BW) method applied to the *full* system (59)–(60) and (61), for different truncation orders L. The modes are insensitive to the truncation order within the quoted numerical accuracy.

By applying the Breit-Wigner method we have numerically verified the argument given in Sec. II, i.e. that the $\ell\to\ell\pm1$ couplings do not affect the eigenfrequencies in the slow-rotation limit. As an example, in Table I we compare two modes ($m=1$, $\tilde{a}=0.1$, $M\mu=0.1$) of the full system computed with the Breit-Wigner resonance method for several truncation orders L and the same modes computed with a direct integration of the system of equations *without* the $\ell\to\ell\pm1$ couplings. Up to numerical accuracy the mode is insensitive to the truncation order and, most importantly, it agrees very well with that computed for the system without couplings. Note that $L=1$ corresponds to the uncoupled polar system with $\ell=1$. Therefore the small discrepancy is not due to the coupling terms, but to some inherent numerical error of the resonance method, which becomes less accurate when the imaginary part of the mode is tiny.

VI. RESULTS

A. Numerical procedure

In principle, by integrating the full systems (70) and (71) for a given truncation order L and a given value of m one can obtain the full spectrum of quasinormal modes and bound modes for *both* the axial and polar sectors and for any $\ell<L$. We have computed bound states

and QNMs via the Breit-Wigner procedure of Sec. V C. We double-checked the results using two additional, independent techniques, also described above: the continued fraction method and direct integration of the reduced equations (70) and (71). The results agree within numerical accuracy. The Breit-Wigner procedure and the continued fraction method have been implemented up to first order in the rotation parameter; the direct integration, instead, has been extended up to second order in $\tilde{a}$, in order to validate the results of the first-order integration, as we shall discuss below. Furthermore, when $\omega_I \ll \omega_R$ we found very good agreement with the Breit-Wigner method (cf. Table I).

Exploring the full parameter space of the eigenfrequencies at second order in $\tilde{a}$ is numerically demanding. For this reason, in Sec. VI D below we will present a more extensive survey of results at first order, and compare them to the second-order calculation in Sec. VI E in selected cases.

B. A consistency check: massless vector perturbations

As a preliminary test of our method, we have computed the QNMs of massless vector (i.e., electromagnetic) perturbations of a Kerr BH to first order in $\tilde{a}$. These results can be compared with those obtained by solving the Teukolsky equation without imposing the slow-rotation approximation (see e.g. [4]). In the massless limit the axial equation (65) reduces to

$$\frac{d^2 u_{(4)}}{dr_*^2} + \left(\omega^2 - \frac{4\tilde{a}M^2 m\omega}{r^3} - \frac{\ell(\ell+1)}{r^2}F\right) u_{(4)} = 0\,. \quad (91)$$

For the polar sector in the massless limit, we can define exactly the same master variable as in the nonrotating case [74]. The polar sector in the massless limit is described by a fourth-order equation. As in the nonrotating case [16], one solution of this equation is a pure-gauge mode and can be eliminated. In the slow-rotation approximation we can recast the other solution in terms of a master function, which also satisfies Eq. (91). Therefore axial and polar perturbations have the same spectra. This is consistent with the fact that electromagnetic perturbations of the full Kerr geometry are described by a single master equation in the Teukolsky formalism [4].

Due to isospectrality, in the massless limit we only need to solve Eq. (91). The modes can be computed via the continued fraction method introduced above, where the coefficients of the recurrence relation can be obtained by setting $\mu = 0$ and $s = \pm 1$ in Eqs. (80)–(82).

We compared our results with the exact massless vector modes of a Kerr BH, computed by solving the Teukolsky equation, for $\ell = 1$ and different values of m (see Fig. 2). The first order approximation performs very well, even for relatively large values of the BH rotation rate. Remarkably, the real and imaginary parts of the QNMs computed with our approach deviate by less than 1% from their exact values if $\tilde{a} \lesssim 0.3$.

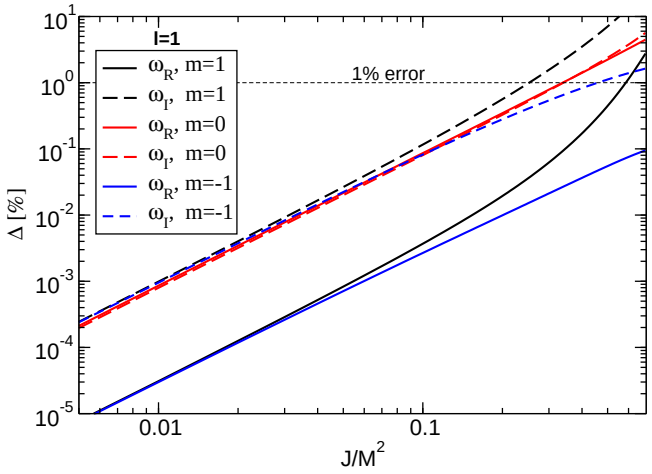

FIG. 2. (color online) Percentage difference between QNMs of massless vector perturbations in the slow-rotation limit at first order and the "full" numerical solution of the Teukolsky equation in the Kerr metric [4]. The deviation scales like $\tilde{a}^2$ as $\tilde{a} \to 0$.

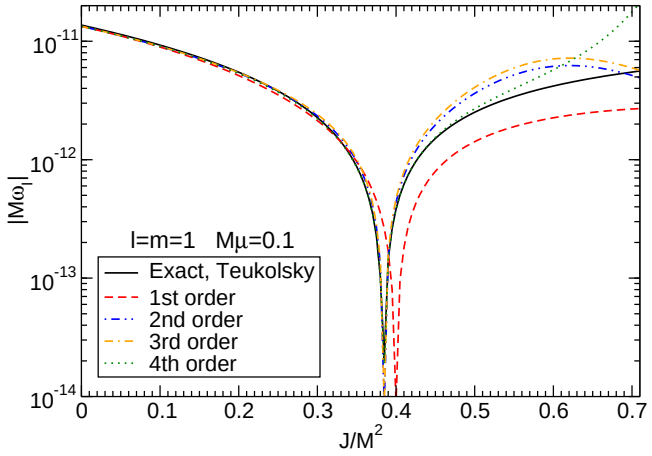

FIG. 3. (color online) Comparison between the exact, Teukolsky-based result and the results obtained by our slowly rotating approximation at first and second order for the imaginary part of the scalar fundamental bound-state mode with $\ell = m = 1$ and $\mu M = 0.1$. For comparison, we have also computed the same mode as obtained by expanding the Teukolsky equation at third and fourth order.

C. A second test: bound state modes for scalar perturbations

We can also investigate the accuracy of the slow-rotation approximation for massive scalar perturbations, another case in which the Teukolsky equation can be

solved exactly (see e.g. [35]). In Fig. 3 we show the imaginary part of the bound state modes with $\ell = m = 1$ and $M\mu = 0.1$, computed by solving Eq. (39) at first and second order via direct integration, against the exact Teukolsky-based result obtained with the continued fraction method [4, 35]. For comparison, we also show the results obtained by solving Teukolsky's equation at third and fourth order. As shown in Fig. 3, the imaginary part crosses the axis when the superradiant condition is satisfied. In the stable branch ($\tilde{a} \lesssim 0.4$) even first-order results are in good quantitative agreement with the "exact" calculation. In the unstable branch ($\tilde{a} \gtrsim 0.4$) the first-order approximation is in only qualitative agreement with the exact result, but the second-order approximation is in quantitative agreement with the numerics at the onset of the instability. It is still quite remarkable that even first-order results can correctly reproduce the onset of the instability. We shall return to this consideration below, when we will deal with the massive vector case.

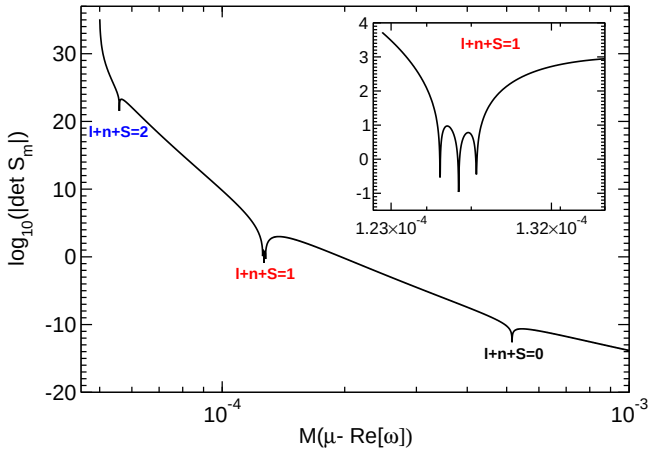

FIG. 4. (color online) Bound state modes obtained with a first-order Breit-Wigner method applied to the full system. We show the determinant $|\det \mathbf{S}_m|$ as a function of the real part of the frequency for $M\mu = 0.1$ and $\tilde{a} = 0.1$. According to Eq. (93), the real part of modes with the same $\ell + n + S$ is approximately degenerate for $M\mu \ll 1$.

D. Proca modes to first order

Unlike the massless case, axial and polar modes for massive vector perturbations are not isospectral. Furthermore there exist two classes of polar modes, which can be distinguished by their "polarization" [16]. For small $M\mu$, Rosa and Dolan found that the imaginary part of the bound states of a Schwarzschild BH scales as

$$\omega_I \sim \mu (M\mu)^{4\ell+5+2S} , \tag{92}$$

where $S = 0$ for axial modes and $S = \pm 1$ for the two classes of polar modes. The monopole corresponds to $\ell = 0$, $S = 1$, in agreement with the rules for addition of angular momenta [16]. In the limit $\tilde{a} = 0$ we recover this scaling. We have also analyzed the $\tilde{a}$-dependence of the modes for small $\tilde{a}$. When $M\mu \ll 1$ we find the expected hydrogen-like behavior, $\omega_R \sim \mu$, which remains valid also in the slowly rotating case. When $M\mu \lesssim 0.1$ the real part of the modes is roughly independent of $\tilde{a}$, and it is very well approximated by the relation

$$\omega_R^2 = \mu^2 \left[1 - \left(\frac{M\mu}{\ell + n + S + 1} \right)^2 \right] + \mathcal{O}\left(\mu^4\right) , \tag{93}$$

where $n \geq 0$ is the overtone number (cf. [35]). For the axial case ($S = 0$) this relation is validated by the analytical results presented in Appendix C [see in particular Eq. (C9)], where we solve the axial equations in the limit $M\mu \ll 1$. Equation (93) is also supported by the nonrotating result given in Eq. (49) of [16] (see also [53]).

Equation (93) predicts a degeneracy for modes with the same value of $\ell + n + S$ when $M\mu \ll 1$. In the Breit-Wigner method, the mode frequencies can be identified as minima of the real-valued function $|\det \mathbf{S}_m|^2$. The degeneracy predicted by Eq. (93) is not exact for $M\mu = 0.1$, as illustrated in the inset of Fig. 4, where we display the minima of $|\det \mathbf{S}_m|^2$ when $\tilde{a} = 0.1$. The first minimum on the right corresponds to $\ell + n + S = 0$, which can only be achieved for the fundamental polar mode with $(\ell, n, S) = (1, 0, -1)$. When $\ell + n + S = 1$ we have a three-fold degeneracy, corresponding to $(\ell, n, S) = (1, 0, 0)$, $(2, 0, -1)$, $(1, 1, -1)$. The approximate nature of the degeneracy is shown in the inset, where three distinct (albeit very close) minima appear. For $\ell + n + S = 2$ there is a five-fold degeneracy, which can be resolved with high enough resolution. Note that according to Eq. (95) the imaginary part of the modes is tiny when $\ell + n + S$ is large. This makes it difficult to numerically resolve higher overtones and modes with large ℓ.

The imaginary part of nonaxisymmetric modes shows the typical Zeeman-like splitting for different values of m when $\tilde{a} \neq 0$, as shown in Fig. 5 for the axial modes and for the polar mode with $S = -1$. For $m > 0$ the imaginary part of the frequency decreases (in modulus) as $\tilde{a}$ increases, and it has a zero crossing when

$$\omega_R \sim \mu = m\Omega_H \sim m\frac{\tilde{a}}{4M} + \mathcal{O}(\tilde{a}^3) , \tag{94}$$

which according to Eq. (74) corresponds to the onset of the superradiant regime. Recall that a second-order calculation is needed to describe the superradiant regime in a self-consistent way, because the latter is well beyond the nominal regime of validity of the first-order approximation. It is quite remarkable that even the first-order approximation predicts that the instability should "turn on" at the right point, as shown in Fig. 6 for $\ell = m = 1$ and several values of μ. The quantitative accuracy of the first-order approximation is questionable in the superradiant regime. However, we will now show that second-order results indicate that we are correctly capturing the

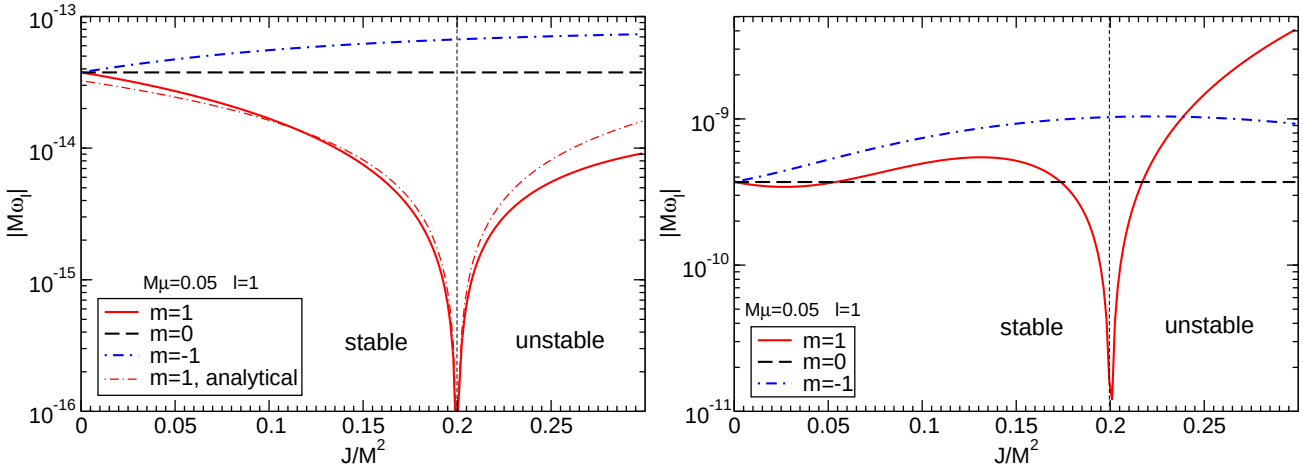

FIG. 5. (color online) Absolute value of the imaginary part of the axial (left panel) and of the polar $S = -1$ (right panel) vector modes as a function of the BH rotation rate $\tilde{a}$ for $\ell = 1$, $M\mu = 0.05$ and different values of m, computed at first order. For $m = 1$, the modes cross the axis and become unstable when the superradiance condition (94) is met. In the left panel, the red dot-dashed line denotes the analytical result (C12).

order of magnitude of the instability even for moderately large rotation.

E. Proca modes to second order

As discussed in Sec. IV C, the perturbation equations for massive vector fields at second order in rotation, Eqs. (70) and (71), are obtained from Eqs. (69), using the perturbation equations in the nonrotating limit to eliminate the second derivatives. The explicit form of the equations is available online [61].

Solving the eigenvalue problem for these equations is numerically more demanding than in the case of perturbations at first order in $\tilde{a}$, especially when the imaginary part of the modes is tiny (as in the axial case and in the small-mass limit). For this reason we present only a selection of results that allow us to validate the accuracy of the first-order approximation, and (more in general) to estimate the errors due the slow-rotation approximation.

The imaginary part of the fundamental $S = 0$ axial and $S = -1$ polar modes as a function of $\tilde{a}$ at first and second order are shown in Fig. 7. The slow-rotation method correctly predicts the onset of the Proca instability already at first order, where (a priori) large deviations could be expected. Furthermore, the value of $\tilde{a}$ which corresponds to the onset of the instability is slightly smaller at second order, consistently with the fact that the horizon location gets negative second-order contributions [cf. Eq. (19)]. Fig. 7 actually displays a remarkably good quantitative agreement between the first- and second-order calculations. The main difference is that in the superradiant region the instability predicted by the first-order expansion is *weaker* (by a factor of a few) than the instability computed at second order. Another important point is that our perturbative approach can consistently describe the superradiant regime as long as $M\omega \ll 1$ and $\tilde{a} \ll 1$. Due to the hydrogen-like spectrum of the bound states, this means that we are limited to considering small values of μM. Again, this expectation is validated by Fig. 7.

At second order, all curves in Fig. 7 show a maximum at large values of the spin. This maximum is an artifact of the second-order approximation: a similar feature appears also in the scalar case in which the exact, Teukolsky-based result is monotonic (cf. Fig. 3). In what follows we have discarded numerical data beyond such maxima, and we have taken this truncation into account when estimating numerical errors.

The bottom line of this discussion is that the first order calculation provides a reliable estimate of the order of magnitude of the instability. The second-order calculation should be *quantitatively* reliable even in the unstable regime, at least up to moderately large values of $\tilde{a}$. Roughly speaking, the reason why the first-order calculation captures the correct qualitative properties of the instability can be traced back to the fact that the superradiant instability condition $\omega < m\Omega_H$ is a "first order effect". Because Ω_H is an odd function of $\tilde{a}$, a first-order approximation of this relation can be expected to be valid modulo third-order corrections.

F. The minimum instability growth scale

The agreement between first- and second-order calculations can be used to estimate the order of magnitude of the instability by extrapolation. We will fit our data at the onset of the instability, and then extrapolate to the superradiant region. This procedure should give us at least a correct order of magnitude for the instability timescale. We expect the extrapolation to work better in the axial case, where bound-state frequencies have a

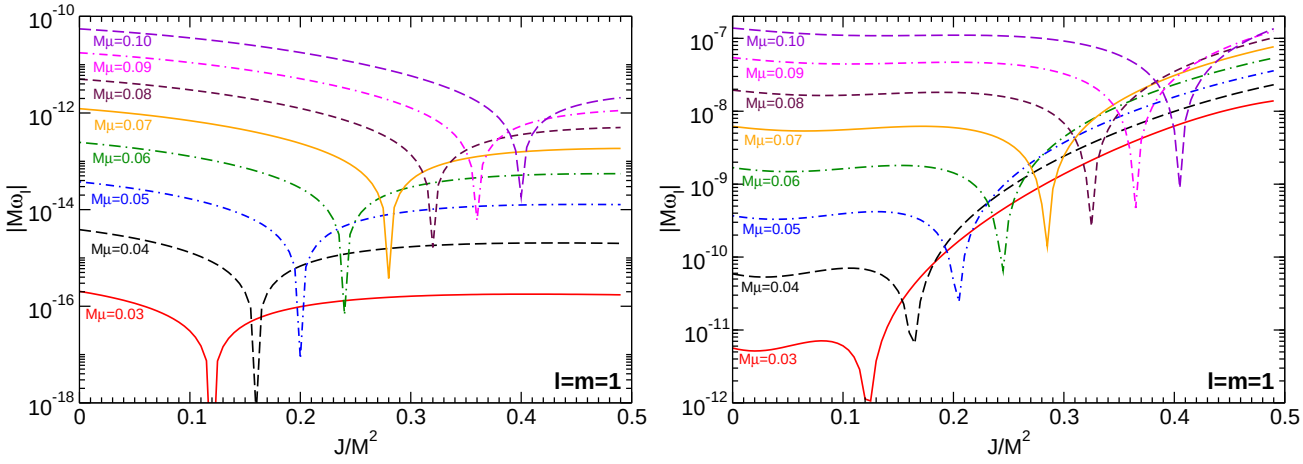

FIG. 6. (color online) Imaginary part of the axial (left panel) and of the polar $S=-1$ (right panel) vector modes as a function of the BH rotation rate $\tilde{a}=J/M^2$ for $\ell=m=1$ and several values of μ. Although beyond the regime of validity of the first order approximation, the modes cross the axis and become unstable precisely when the superradiance condition (94) is met. As shown in Fig. 7, the first-order results are also in qualitatively good agreement with those obtained at second order.

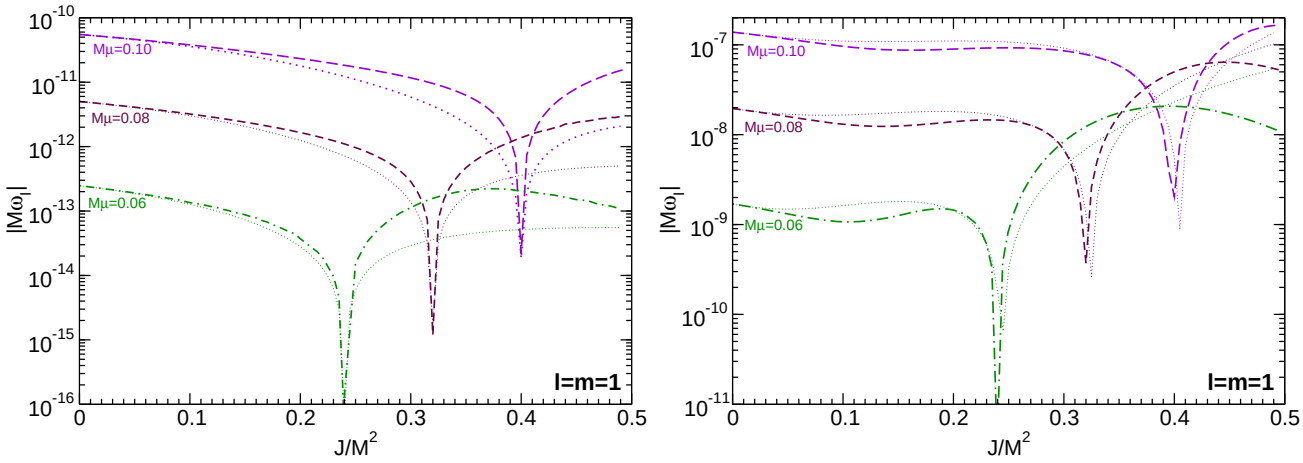

FIG. 7. (color online) Imaginary part of the axial $S=0$ vector modes (left panel) and for polar $S=-1$ vector modes (right panel) computed at second order in the rotation for $\ell=m=1$ and several values of μ. The dotted thinner lines refer to the first order calculation. The modes cross the axis and become unstable when the superradiance condition is met.

monotonic behavior as functions of $\tilde{a}$ (cf. the left panel of Fig. 6). We estimate that close to the onset of the superradiant instability the imaginary part of the modes should scale as follows:

$$M\omega_I \sim \gamma_{S\ell}\,(\tilde{a}m-2r_+\mu)\,(M\mu)^{4\ell+5+2S}\,, \qquad (95)$$

where $\gamma_{S\ell}$ is a coefficient that depends on S and ℓ. For axial modes with $\ell=1$ our numerical data yield $\gamma_{01}\approx 0.09\pm0.03$, in good agreement with the analytical formula in the limit $M\mu\ll 1$,

$$M\omega_I^{(\ell=1\,,\,\mathrm{axial})}=\frac{1}{12}\,(\tilde{a}m-2r_+\mu)\,(M\mu)^9\,, \qquad (96)$$

which is derived in Appendix C. From the equation above we get $\gamma_{01}=1/12\sim 0.0833$. Expression (96) is compared to the numerical results in Fig. 5.

Here and in the following, numerical errors are estimated by comparing the results at first and second order, and by taking the maximum deviation between the fit and the data. We generate numerical data with increasing accuracy until convergence is reached. In particular, in the direct-integration method it is important to retain a sufficiently large number of terms in the series expansion of the boundary condition at infinity, Eq. (77), in order to achieve sufficient accuracy. This is expected because bound-state modes decay exponentially, and therefore it is challenging to perform a numerical integration at large distances.

We have applied the same method to compute unstable massive *scalar* modes [60], whose imaginary part scales as in the case of axial vector modes with $S=0$. In this

case we find $\gamma_{01}^{\rm scalar} \approx 0.03 \pm 0.01$, again in reasonable agreement with analytical expectations (by setting $s = 0$ in Eq. (96) we get $\gamma_{01}^{\rm scalar} = 1/48 \sim 0.0208$). Computing the modes in the limit $M\mu \ll 1$ is numerically challenging because of the steep scaling of ω_I with $M\mu$ [cf. Eq. (95)] and this affects the precision of the fit. Despite these numerical difficulties, we are able to recover the correct order of magnitude for the instability timescale when $M\mu \ll 1$. In any case, the observational bounds that we will address in the next section depend only mildly on the precise value of $\gamma_{S\ell}$. For the polar modes we find $\gamma_{-11} \approx 20 \pm 10$, while extracting the coefficient γ_{11} with sufficient precision is numerically challenging even for the fundamental mode with $\ell = 1$, since $\omega_I \sim (M\mu)^{11}$.

Obviously our method becomes inaccurate when $\tilde{a} \to 1$, and the fit (95) can provide at most an order of magnitude for the instability timescale in the extremal limit. However, in the massive scalar case Eq. (95) with $S = 0$ is *exact* in the $M\mu \ll 1$ limit, for any value of $\tilde{a}$ [60]. Furthermore, in the massive vector case, the good agreement between the first- and second-order expansions suggests that the slow-rotation approximation should be quite accurate even for moderately large spins, $\tilde{a} \lesssim 0.7$. Therefore it is reasonable to expect that extrapolations of Eq. (95) from the slow-rotation limit should at least provide the correct order of magnitude (and possibly a reasonable quantitative estimate) of the instability timescale.

It is tempting to extrapolate our predictions to generic values of $\tilde{a}$ and to discuss possible astrophysical implications of the superradiant instability for massive vector fields around Kerr BHs. Our conclusions rely on extrapolation, so they should be confirmed by independent means. Let us assume that the imaginary part of the modes is generically described by Eq. (95), where we left the coefficient $\gamma_{S\ell}$ undetermined, since its precise value (whose order of magnitude approximately ranges between 0.1 and 10, depending on S and ℓ) is not crucial for the following discussion. From Eq. (95) we find that the instability growth timescale has a minimum (i.e., ω_I has a maximum) for

$$\mu^{\rm min} = m\tilde{a}\frac{5+4\ell+2S}{4r_+(3+2\ell+S)}\,, \tag{97}$$

and the corresponding value of the timescale $\tau = \omega_I^{-1}$ is given by Eq. (95) evaluated at $\mu = \mu^{\rm min}$. From Eq. (95) we also see that (excluding the case $\tilde{a}m \simeq 2r_+\mu$) this is a typical value of the instability timescale.

If we apply the same procedure to scalar fields ($\ell = 1$, $S = 0$, $\gamma_{01}^{-1} = 48$), we find that the minimum instability corresponds to $\tilde{a} = 1$, $M\mu^{\rm min} = 0.45$ and $M\omega_I^{\rm max} = 1.6 \times 10^{-6}$. Notice that this simple argument relies on an (a priori unjustified) extrapolation of analytical expressions valid for $M\mu \ll 1$ to the regime $M\mu \sim 1$. In the scalar case this prediction overestimates the numerical results by an order of magnitude: in fact, Refs. [34, 35] found a minimum instability $M\omega_I \sim 1.5 \times 10^{-7}$ at $M\mu \sim 0.42$ for $\tilde{a} \sim 0.99$. This disagreement should not be surprising. Actually, Eq. (95) performs remarkably well even for values of $\tilde{a}$ close to extremality [43]: it overestimates the results in Table III in Ref. [35] by only 3% when $\tilde{a} = 0.7$ and by less than 70% when $\tilde{a} = 0.99$. In our view, this agreement is quite impressive.

Let us apply the same argument to vector fields. From Eq. (95) we expect the stronger instability when $\ell = m = 1$. For $\tilde{a} = 0.7$ this corresponds to

$$\begin{aligned} &M\mu^{\rm min} \sim 0.187\,, \quad M\omega_I^{\rm max} \sim 5.8\gamma_{11} \times 10^{-10}\,, \\ &M\mu^{\rm min} \sim 0.184\,, \quad M\omega_I^{\rm max} \sim 1.7\gamma_{01} \times 10^{-8}\,, \\ &M\mu^{\rm min} \sim 0.179\,, \quad M\omega_I^{\rm max} \sim 5.1\gamma_{-11} \times 10^{-7}\,, \end{aligned}$$

for $S = 1, 0, -1$, respectively. Our data at second order are compatible with $\gamma_{01} \approx 0.09$ and $\gamma_{-11} \approx 20$. As we discussed, we could not extract the coefficient γ_{11} with sufficient precision. Nevertheless it is not difficult to show that the modes with $S = 1$ are indeed those with the smallest (in modulus) imaginary part, i.e. they are the least interesting for what concerns the instability. This confirms the expectation that polar perturbations with $S = -1$ should have the strongest instability in the rapidly rotating limit, as conjectured in Ref. [16]. In the Proca case the strongest instability should occur on a timescale

$$\tau_{\rm vector} = \omega_I^{-1} \sim \frac{M(M\mu)^{-7}}{\gamma_{-11}(\tilde{a} - 2\mu r_+)}\,. \tag{98}$$

The timescale above must be compared with that for the massive scalar case [60] for $\ell = m = 1$,

$$\tau_{\rm scalar} \sim \frac{48M(M\mu)^{-9}}{\tilde{a} - 2\mu r_+}\,. \tag{99}$$

Roughly speaking, the instability timescale against vector polar perturbations is of order $\tau_{\rm vector} \sim 10^{-2}\gamma_{-11}^{-1}(M/M_\odot)\,{\rm s}$.

In the next section we shall use the results obtained from our numerics at second order to discuss some important astrophysical consequences of the Proca instability. In this context it is crucial to have a robust estimate of the instability timescale in the $M\mu \ll 1$ limit. In the axial case our numerical results are supported by the analytical formula (96), which provides strong support that the fit (95) represents the correct behavior when $M\mu \ll 1$. Unfortunately in the polar case we do not have the same analytical insight and, as discussed above, the small-mass regime is challenging to investigate numerically. In order to verify the reliability of Eq. (95) for polar perturbations we have tried several choices of the fitting functions in the most relevant case, $\ell = m = 1$ and $S = -1$. It turns out that Eq. (95) is a conservative choice in the polar case, as other fits generically predict a *stronger* instability. Furthermore, by comparing the results in Figs. 6 and 7 for the axial and for the polar case, it is clear that the polar case exhibits a more complex behavior, which is hard to reproduce without some analytical insight. In fact our numerical data are also very

well reproduced by the following fitting function:

$$M\omega_I \sim (\tilde{a}-\tilde{a}_{\rm SR})\left[\eta_0(M\mu)^{\kappa_0}+\eta_1\tilde{a}(M\mu)^{\kappa_1}\right]\,, \qquad (100)$$

where

$$\tilde{a}_{\rm SR}=\frac{-m+\sqrt{m^2+16(M\mu)^2}}{2\mu M}\sim\frac{4M\mu}{m}+\mathcal{O}(\mu^3)\,, \quad (101)$$

corresponding to the superradiance threshold [Eq. (94)] when $\omega_R\sim\mu$. The fit (100) has been obtained by imposing a second-order (in $\tilde{a}$) functional form and $\omega_I=0$ when $\tilde{a}=\tilde{a}_{\rm SR}$, consistently with our data. Finally, the functional dependence on μ of the two remaining terms has been obtained by fitting the data in the instability region and for $0.03\lesssim M\mu\lesssim 0.1$. We found $\eta_0\approx-6.5\pm2$, $\eta_1\approx 2.1\pm1$, $\kappa_0\approx 6.0\pm0.1$ and $\kappa_1\approx 5.0\pm0.3$. While the fit (95) is physically more appealing [16], Eq. (100) reproduces our numerical data in the whole instability region within a factor of two. It would be interesting to better understand the behavior of the polar instability in the limit $M\mu\ll 1$ using different approaches, such as a time-evolution analysis or a full numerical evolution of the Proca equation. In the following we shall discuss how the choice of either Eq. (95) or Eq. (100) affects the astrophysical implications of our results.

VII. ASTROPHYSICAL IMPLICATIONS OF THE PROCA INSTABILITY

Our numerical results in the previous section indicate that polar perturbations with $S=-1$ have the shortest instability timescale, as conjectured in [16]. For fixed values of $\tilde{a}$ and μ, the instability timescale for polar perturbations is smaller by two-three orders of magnitude than in the axial case. While this conclusion relies on an extrapolation of calculations that are valid (strictly speaking) only in the slow-rotation limit, we have shown that a similar extrapolation in the scalar case is in remarkable quantitative agreement with numerical results that do *not* rely on the slow rotation approximation. Furthermore, in the Proca case a second-order calculation gives solid evidence that our extrapolation is reliable, both qualitatively and quantitatively. Therefore it is reasonable to expect that extrapolations from the slow-rotation limit should at least provide the correct order of magnitude (and possibly a reliable quantitative estimate) of the polar instability timescale. Here we explore the tantalizing astrophysical implications of the Proca superradiant instability. Unless otherwise stated, we shall focus on the most relevant modes, those with $\ell=m=1$, which correspond to the stronger instability.

A. Implications from the existence of supermassive black holes

The most conservative assumption on the final state of the instability is that the radiation will extract angular momentum from the BH, leaving behind a Kerr metric with dimensionless spin parameter below the superradiant threshold: in other words, the angular frequency of the BH horizon must be such that $\Omega_H\lesssim\mu$. By this argument, even a single reliable supermassive BH spin measurement can impose a stringent constraint on the allowed mass range of massive vector fields. Bounds on the mass of the vector field follow from the requirement that astrophysical spinning BHs should be stable, in the sense that the timescale (98) should be larger than some observational threshold.

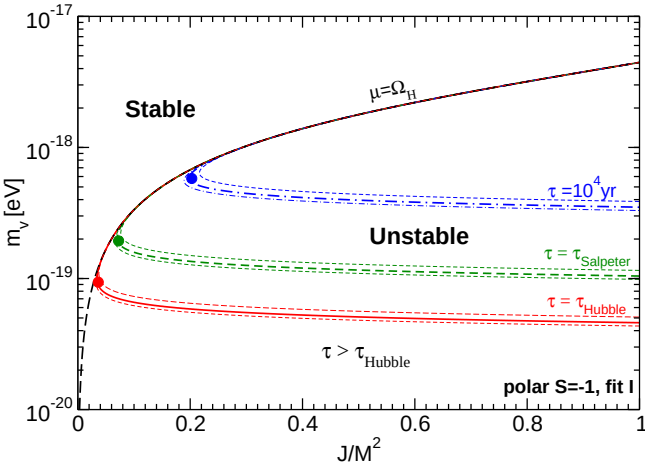

FIG. 8. (color online) Bounds on the photon mass $m_v=\hbar\mu$ obtained by extrapolating the instability timescale (98) for $S=-1$ polar Proca modes of a Kerr BHs up to $\tilde{a}=1$. The region delimited by the curves corresponds to an instability timescale $\tau<\tau_{\rm Hubble}$ (continuous red line), $\tau<\tau_{\rm Salpeter}$ (dashed green line) and $\tau<10^4$ yr (dot-dashed blue line), respectively. We set $\gamma_{-11}\approx 20\pm10$ in Eq. (98) and consider a Kerr BH with $M=10^7M_\odot$, but the results have a simple scaling with γ_{-11} and with the BH mass (cf. Eqs. (102) and (103)). Thin dashed lines bracket our estimated numerical errors.

For isolated BHs we can consider the observational threshold to be the age of the Universe, $\tau_{\rm Hubble}=1.38\times10^{10}$ yr. A more conservative assumption is to include possible spin growth due to mergers with other BHs and/or accretion. These effects are in competition with superradiant angular momentum extraction.

The most likely mechanism to produce fast-spinning BHs[3] is prolonged accretion [78]. In this case we can compare the superradiance timescale to the shortest

[3] Supermassive BHs with moderate spin (say $\tilde{a}\sim0.7$, as in Fairall 9 [57]) could also be produced by comparable-mass BH mergers [9]. The timescale for mergers depends on details of the "final parsec problem", which are poorly known [75]. The *minimum* timescale necessary for BHs to merge is the gravitational-radiation timescale, which is of the same order as the Salpeter timescale (cf. Eq. (10) in [75] or Eq. (26) in [76]), but it is likely that the timescale for binary BHs to merge will be dominated by

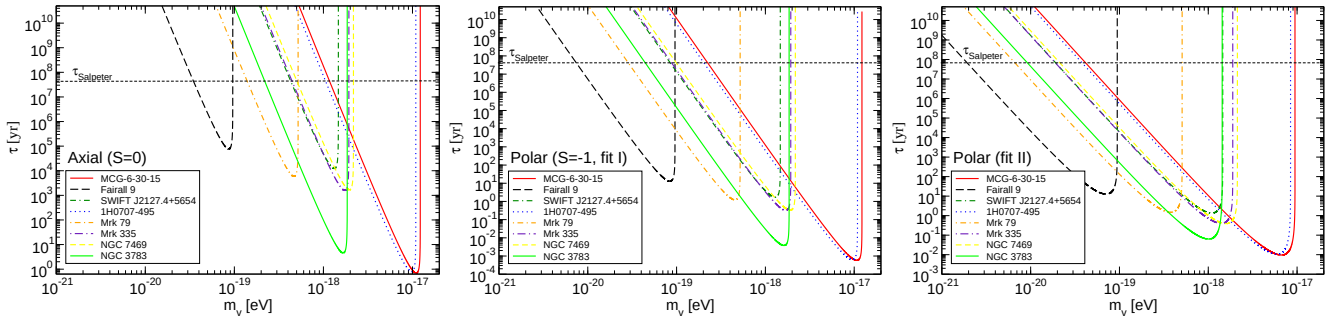

FIG. 9. (color online) Instability timescale (in years) as a function of the vector mass m_v (in eV) for the eight supermassive BHs listed in Table 2 of [56]. The left panel refers to the axial case ($S = 0$, $\ell = m = 1$); the middle panel to the polar case, Eq. (95) with $S = -1$, $\ell = m = 1$ and $\gamma_{-11} \approx 20$; the right panel to the polar case, but using the alternative fitting function given in Eq. (100). The horizontal line corresponds to $\tau = \tau_{\rm Salpeter} = 4.5 \times 10^7$ yr.

timescale over which accretion could spin up the BH. Thin-disk accretion can increase the BH spin from $\tilde{a} = 0$ to $\tilde{a} \approx 1$ with a corresponding mass increase by a factor $\sqrt{6}$ [79]. If we assume that mass growth occurs via accretion at the Eddington limit, so that the BH mass grows exponentially with e-folding time given by the Salpeter timescale $\tau_{\rm Salpeter} = 4.5 \times 10^7$ yr, then the *minimum* timescale for the BH spin to grow from $\tilde{a} = 0$ to $\tilde{a} \approx 1$ via thin-disk accretion is comparable to $\tau_{\rm Salpeter}$. Note that accretion at the Eddington limit is a rather conservative assumption, since more typically we would expect accretion to be sub-Eddington. Furthermore fast-spinning BHs are hard to produce in the presence of radiative effects [80] or magnetohydrodynamics [81], and "chaotic" accretion [82] would make large spin parameters even less likely.

For illustration, in Fig. 8 we consider a Kerr BH with $M = 10^7 M_\odot$, so that $m_v = 10^{-17}(M\mu)$ eV. We assume $\gamma_{-11} \approx 20 \pm 10$ in Eq. (98) (consistently with our numerical results) and we plot: (i) the superradiant threshold (dashed black line), corresponding to the points where $\mu \approx \Omega_H$ and the instability timescale (in the perturbative treatment) becomes infinite; (ii) the contours corresponding to an instability timescale $\tau = \tau_{\rm Hubble}$ (continuous red line), $\tau = \tau_{\rm Salpeter}$ (dashed green line) and $\tau = 10^4$ yr (dash-dotted blue line), respectively. Each curve is shown with the corresponding error bars.

In the region delimited by the continuous red line the instability timescale is shorter than the Hubble time (of course, similar considerations apply to the dashed green and dash-dotted blue lines). For large $\tilde{a}$ the lower branches of the "critical" curves are roughly horizontal. By solving $\omega_I^{-1} = \tau_c$ in the limit $M\mu \ll 1$ this regime can be well approximated by the formula

$$m_v^* = \hbar\mu^* = \frac{\hbar}{M}\left[\frac{M}{m\gamma_{S\ell}\tau_c}\right]^{1/(5+4\ell+2S)} , \qquad (102)$$

where τ_c is the threshold time. If $\tau_c = \tau_{\rm Hubble}$ and in the $S = -1$ polar case, we get

$$m_v^* \sim \frac{7\times 10^{-20}}{\gamma_{-11}^{1/7}}\left[\frac{10^7 M_\odot}{M}\right]^{6/7} {\rm eV}\,. \qquad (103)$$

Note that, although extracting the values of the fitting parameters can be numerically challenging, our results depend very mildly on the precise value of γ_{-11}. From Eq. (98) we see that the instability timescale is inversely proportional to γ_{-11}. Therefore the near-horizontal "observability threshold" in Fig. 9 that would correspond to choosing $\tau = \tau_{\rm Salpeter}$ rather than $\tau = \tau_{\rm Hubble}$ can be obtained multiplying γ_{-11} in Eq. (103) by the ratio of the two timescales, $\tau_{\rm Salpeter}/\tau_{\rm Hubble} \simeq 3 \times 10^{-3}$. Then the vector mass bound (103) would increase by a modest factor of 2.3. What is crucial in obtaining strong astrophysical bounds is having a large BH mass, because bounds scale like $\left(10^7 M_\odot/M\right)^{6/7}$.

Brenneman et al. [56] have recently presented a list of eight supermassive BH mass and spin estimates. In Fig. 9 we show the superradiant instability timescale τ (in years) as a function of m_v (in eV) for these supermassive BHs. The dashed horizontal line denotes $\tau_{\rm Salpeter}$, which we (conservatively) assume as the threshold for the timescale to be observationally significant. For each system we compute instability timescales using the BH mass and spin estimates given in Table 2 of [56] (we select either the average spin value quoted in the table, or the lower limit on the spin when the observations imply $\tilde{a} > 0.98$). The left panel refers to axial modes with $S = 0$ and $\ell = m = 1$, for which we can compute the instability timescale analytically: cf. Eq. (96) and Appendix C. The middle and right panels shows that qualitatively similar results hold for polar modes with $S = -1$ and $\ell = m = 1$, which exhibit the strongest instability.

the dynamical friction timescale, which is typically of the order of a few Gyrs for satellites in a Milky Way-type halo [77] and hence larger than the Salpeter timescale.

In the polar case, we computed the instability timescale using both Eq. (95) (fit I) and Eq. (100) (fit II). The results are qualitatively similar and show that, independently of the fitting function, the axial bounds on m_v are typically one-two orders of magnitude less stringent than the polar bounds. Fig. 9 shows that *existing* measurements of supermassive BH spins rule out Proca field masses in the whole range 10^{-20} eV$\lesssim m_v \lesssim 10^{-17}$ eV.

Note that arguments based on the superradiant instability can only be used to set "exclusion windows" on the boson mass, rather then upper bounds [42, 43]. However, observations of BHs in different mass ranges can exclude different mass windows. For example, stellar-size BHs, $M \simeq (5-20)M_\odot$, can set an exclusion region of 10^{-13} eV$\lesssim m_v \lesssim 10^{-9}$ eV. This mass range is relevant for so-called "dark photons" coupled to sterile neutrinos [83]. If the identified intermediate-mass BHs were confirmed to exist and if the largest known supermassive BHs with $M \simeq 2\times 10^{10} M_\odot$ [84, 85] were confirmed to have sufficiently large spin, combined observations of spinning BHs can potentially exclude the entire mass windows 10^{-21} eV$\lesssim m_v \lesssim 10^{-9}$ eV [42, 43]. The latter is complementary to the bounds set by several other experiments and observations that exclude light bosonic particle with larger mass [52, 83, 86].

Using current data on supermassive BHs [56], the best bound comes from Fairall 9 [57], for which the polar instability implies a conservative bound (including measurement errors) $m_v \lesssim 10^{-20}$ eV or $m_v \lesssim 10^{-21}$ eV, depending on the fitting function [59]. Although the instability for axial modes is weaker, in this case our results are more precise and imply a bound as stringent as $m_v \lesssim 4\times 10^{-20}$ eV if we consider $\tau < \tau_{\rm Salpeter}$, or $m_v \times 10^{-20}$ eV if we consider $\tau < \tau_{\rm Hubble}$. Even under our very conservative assumptions these results are of great significance, since the current best bound on the photon mass is $m_\gamma < 10^{-18}$ eV [52, 86]. Combining the exclusion window derived above, $10^{-20}\lesssim m_v \lesssim 10^{-17}$ eV, with existing bounds [52, 86], we find the most stringent upper bound on the photon mass, $m_\gamma \lesssim 10^{-20}$ eV.

We remind the reader that our results are also summarized in Fig. 1, where we show instability windows for axial and polar modes together with supermassive BH mass and spin estimates from Ref. [56].

B. Nonlinear effects, other couplings

An important ingredient that was not taken into account in our study is the nonlinear evolution of the instability, that can modify the background geometry. Photon self-interactions are very weak, being suppressed by the mass of the electron. Therefore, it is quite likely that the outcome of the instability will be a slow and gradual drainage of the hole's rotational energy. However, exotic massive vector fields may show nonlinearities as those studied in Ref. [46, 47] for the scalar case.

Another important aspect that should be investigated is whether the coupling of accreting matter to massive bosons can quench the instability. In principle massive photons (unlike hidden $U(1)$ fields, for which the interaction with matter is very small) can couple strongly to matter. However it is unlikely that this will significantly affect the superradiant instability discussed here, for two reasons. The first is that unstable modes are large-scale coherent modes whose Compton wavelength is comparable to (or larger than) the size of the BH's event horizon, and accretion disks are typically charge-neutral over these lengthscales, so any possible coupling with ordinary neutral matter is incoherent and most likely inefficient. The second is that accretion disks are expected to be localized on the equatorial plane, and therefore can affect at most some (but not all) of the unstable modes. The investigation of the superradiant instability in the presence of matter requires further work, but the above considerations suggest that vacuum estimates should be reliable. Spin estimates for slowly accreting BHs (such as the BH at the center of our own galaxy) are the most reliable, in that they should be less sensitive to details of the interaction of vector fields with matter.

VIII. CONCLUSIONS AND EXTENSIONS

BH perturbation theory is a powerful tool, with important applications in astrophysics and high-energy physics, but its applicability is limited when the perturbation equations cannot be separated. We have discussed a general method to circumvent these difficulties in the case of slowly rotating BH spacetimes. The method was originally developed to study the modes of rotating stars but, as we showed, it applies to *any* slowly rotating BH background and to any kind of perturbation. Within this general framework, we discussed two effects induced by rotation: (i) the Zeeman-like splitting of the eigenfrequencies, that breaks the degeneracy of modes with different azimuthal number m, and (ii) a Laporte-like selection rule, in which modes with multipolar index ℓ are coupled to those with multipolar index $\ell\pm 1$ and opposite parity and to those with $\ell\pm 2$ and same parity. We have extended Kojima's arguments to show that these couplings do not affect the QNM frequencies of the spacetime to first order in the rotation rate, and we verified this claim by numerical integration of the perturbation equations.

As a first relevant application of this method, we studied massive vector (Proca) perturbations on a slowly rotating Kerr background, i.e. the only interesting class of perturbations of Kerr BHs in four dimensions that does not seem to be separable. Using our approach we reduced the equations to a set of coupled ODEs, that can be solved by a straightforward extension of methods valid in the nonrotating case. We have computed the corrections to the Proca eigenfrequencies of a Kerr BH to first and to second order in the rotation rate. For the first time we showed that the Proca bound-state modes become unstable when the superradiant condition (74)

is met. We proved this numerically for the polar modes, and both numerically and analytically for the axial modes in the limit $M\mu \ll 1$. Unfortunately the method becomes intrinsically inaccurate for large values of the rotation rate. This prevents us from accurately computing the instability timescale close to extremality. By fitting and extrapolating our data we confirmed the scaling with m_v conjectured in Ref. [16], and we also estimated the order of magnitude of the instability timescale. We expect our results to be reliable up to $\tilde{a} \sim 0.7$. Our estimates should be confirmed by more accurate methods, but they provide strong evidence that measurements of rotating supermassive BH spins set the most stringent upper bounds on the photon mass (cf. Fig. 1).

Besides their astrophysical implications, our results are relevant also for some classes of gravitational theories with higher-order curvature terms in the action. For example, as proved by Buchdahl [87], a theory defined by $\mathcal{L} = \sqrt{-g}\left(R + \alpha R_{[ab]}R^{[ab]}\right)$ in the Palatini approach is dynamically equivalent to the Einstein-Proca system when the vector mass $\mu^2 = 3/|\alpha|$ (see also Ref. [88]). The Proca instability of Kerr BHs in this theory can put constraints on the parameter α, which is related to the nonmetricity of the connection.

While limited by the slow-rotation assumption, the power of the present method consists in its generality. The slow-rotation approximation allows us to study linear perturbations of any slowly rotating spacetime even when the equations are nonseparable. For instance it can be used to study gravitational-electromagnetic perturbations of Kerr-Newman BHs in four dimensions [12], QNMs of Myers-Perry BHs [14] and BH greybody factors in higher-dimensional rotating spacetimes [11, 54]. Another interesting extension is the stability analysis of rotating BHs in asymptotically anti-de Sitter spacetimes. This is relevant in the context of the gauge/gravity duality, as the QNMs of anti-de Sitter BHs in five dimensions are holographically related to specific correlation functions and transport coefficients of the dual boundary theory [4].

We note that perturbations of rotating stars have been studied up to second order in the Cowling approximation (see e.g. Refs. [89–91]), where metric perturbations are neglected and the equations have a structure reminiscent of our general Eqs. (4) and (5).

Finally we remark that the techniques discussed in this paper are not limited to general relativity. They are also useful to study gravitational perturbations and the linear stability of slowly rotating BH metrics in alternative theories of gravity, for example in quadratic gravity [22, 25, 26]. We hope to report on these interesting extensions in the near future.

ACKNOWLEDGMENTS

We wish to thank the Axiverse Project members (especially Hideo Kodama), Antonino Flachi, Stefano Liberati and João Rosa for valuable discussions, and the referees for their constructive comments. This work was supported by the DyBHo–256667 ERC Starting Grant, the NRHEP–295189 FP7–PEOPLE–2011–IRSES Grant, and by FCT - Portugal through PTDC projects FIS/098025/2008, FIS/098032/2008, CTE-ST/098034/2008, CERN/FP/123593/2011. A.I. was supported by JSPS Grant-in-Aid for Scientific Research Fund No. 22540299 and No. 22244030. E.B. was supported by NSF Grant No. PHY-0900735 and NSF CAREER Grant No. PHY-1055103. P.P. acknowledges financial support provided by the European Community through the Intra-European Marie Curie contract aStronGR-2011-298297 and the kind hospitality of the Department of Physics, University of Rome "Sapienza" and of the International School for Advanced Studies (SISSA) in Trieste. V.C. thanks the Yukawa Institute for Theoretical Physics at Kyoto University for hospitality during the YITP-T-11-08 workshop on "Recent advances in numerical and analytical methods for black hole dynamics".

Appendix A: Coefficients of the perturbation equations

In this Appendix we list the explicit form of the coefficients appearing in the perturbation equations. We remark that the coefficients $A_\ell, D_\ell, A_\ell^{(i)}, B_\ell^{(i)}, D_\ell^{(i)}$ incorporate terms at zeroth, first and second order in the rotation parameter $\tilde{a}$. Therefore, there is no direct correspondence between these coefficients and the quantities at fixed order in $\tilde{a}$, such as $\mathcal{A}_\ell$, $\bar{\mathcal{A}}_\ell$, $\hat{\mathcal{A}}_\ell$, etc., which have been introduced in Sec. II. In the following, a prime denotes derivative with respect to the radial coordinate r.

1. Coefficients of the scalar equation

The explicit form of the coefficients appearing in Eq. (22) is

$$\begin{aligned} A_\ell = &-2\left[M^2r^2\left(\left(4M^2+2Mr\left(\Lambda-1+r^2\mu^2\right)+r^4\omega^2\right.\right.\right. \\ &\left.\left.\left.-r^2\left(\Lambda+r^2\mu^2\right)\right)\Psi_\ell + r(r-2M)\left(2M\Psi'_\ell\right.\right.\right. \\ &\left.\left.\left.+r(r-2M)\Psi''_\ell\right)\right)\right] + 8\tilde{a}mM^4r^3\omega\Psi_\ell + \tilde{a}^2M^4\left[\left(36M^2\right.\right. \\ &\left.+2Mr\left(\Lambda-11+r^2\mu^2\right)-r^2\left(\Lambda-2+2m^2+r^2\mu^2\right)\right. \\ &\left.\left.+\frac{r^3\omega^2}{r-2M}\left(8M^2-2Mr+r^2\right)\right)\Psi_\ell\right. \\ &\left.+r(r-2M)\left(10M\Psi'_\ell - r(2M+r)\Psi''_\ell\right)\right], \end{aligned} \tag{A1}$$

$$\begin{aligned} D_\ell = &\,2\tilde{a}^2M^4\left[\left(4M^2-\Lambda r^2+2Mr\left(\Lambda-1+r^2\omega^2\right)\right)\Psi_\ell\right. \\ &\left.+r(r-2M)\left(2M\Psi'_\ell + r(r-2M)\Psi''_\ell\right)\right]. \end{aligned} \tag{A2}$$

2. Coefficients of the Proca perturbation equations

In this Appendix we list the coefficients appearing in Eqs. (44)–(47). The coefficients read

$$
\begin{aligned}
A^{(0)}_\ell = \frac{\tilde{a}^2M^2}{2r^6}\Bigg[&\frac{u^\ell_{(1)}\left(-r^2\left(\Lambda+2m^2+\mu^2r^2-2\right)+32M^2+2Mr\left(\Lambda+\mu^2r^2-10\right)\right)}{2M-r}+\\
&\frac{r}{\ell(\ell+1)(r-2M)^2}\left((2M-r)\left(\ell(\ell+1)(2M-r)\left(-12Mu'^\ell_{(1)}+r(2M+r)u''^\ell_{(1)}+ir^2\omega u'^\ell_{(2)}\right)-2im^2r^2\omega u^\ell_{(3)}\right)\right.\\
&\left.-i\Lambda r\omega\left(-8M^2-2Mr+r^2\right)u^\ell_{(2)}\right)\Bigg]+\frac{2\tilde{a}mM^2\left(\Lambda r\omega u^\ell_{(1)}-i\left((2M-r)u'^\ell_{(3)}-r^2\omega^2u^\ell_{(3)}+\Lambda u^\ell_{(2)}\right)\right)}{\Lambda r^4(2M-r)}\\
&-\frac{(2M-r)\left(\Lambda+\mu^2r^2\right)u^\ell_{(1)}+r(r-2M)^2u''^\ell_{(1)}+ir\omega\left((2M-r)\left(u^\ell_{(3)}-ru'^\ell_{(2)}\right)+(r-4M)u^\ell_{(2)}\right)}{r^3(2M-r)}\,,
\end{aligned}
\tag{A3}
$$

$$
\begin{aligned}
A^{(1)}_\ell = \frac{\tilde{a}^2M^2}{2\Lambda r^4(2M-r)^3}\Big[&\Lambda u^\ell_{(2)}\left((2M-r)\left(\ell^2(2M+r)+\ell(2M+r)+r\left(2m^2+\mu^2r(2M+r)\right)\right)+r^2\omega^2\left(8M^2+2Mr+r^2\right)\right)\\
&+2m^2r(r-2M)^2u'^\ell_{(3)}+i\Lambda r\omega(2M-r)\left(8M^2-2Mr+r^2\right)u'^\ell_{(1)}-i\ell(\ell+1)\omega(2M-r)\left(8M^2-6Mr+3r^2\right)u^\ell_{(1)}\Big]\\
&+\frac{2\tilde{a}mM^2\left(r^2\omega(r-2M)u'^\ell_{(3)}+i\Lambda\left((2M-r)u^\ell_{(1)}+r\left((r-2M)u'^\ell_{(1)}+2ir\omega u^\ell_{(2)}\right)\right)\right)}{\ell(\ell+1)r^4(r-2M)^2}\\
&+\frac{(2M-r)\left((2M-r)u'^\ell_{(3)}+ir^2\omega u'^\ell_{(1)}\right)+u^\ell_{(2)}\left((2M-r)\left(\Lambda+\mu^2r^2\right)+r^3\omega^2\right)-ir\omega(2M-r)u^\ell_{(1)}}{r^2(r-2M)^2}\,,
\end{aligned}
\tag{A4}
$$

$$
\begin{aligned}
A^{(2)}_\ell = &\frac{\tilde{a}^2M^2\left((2M-r)\left(-2m^2ru^\ell_{(3)}-\Lambda r(r-2M)u'^\ell_{(2)}-\Lambda(2M-r)u^\ell_{(2)}\right)-i\Lambda r\omega\left(8M^2-2Mr+r^2\right)u^\ell_{(1)}\right)}{\ell(\ell+1)(r-2M)^2}\\
&+\frac{4\tilde{a}mM^2r(r\omega u^\ell_{(3)}+i\Lambda u^\ell_{(1)})}{\Lambda(2M-r)}+\frac{2r^2\left((2M-r)\left(ru'^\ell_{(2)}+u^\ell_{(2)}-{u_{(3)}}^\ell(r)\right)-ir^2\omega u^\ell_{(1)}\right)}{2M-r}\,,
\end{aligned}
\tag{A5}
$$

$$
\tilde{A}^{(0)}_\ell = \frac{4\tilde{a}M^2u^\ell_{(4)}}{r^5}-\frac{4\tilde{a}^2mM^3\omega u^\ell_{(4)}}{\Lambda r^5}\,,
\tag{A6}
$$

$$
\tilde{A}^{(1)}_\ell = -\frac{2i\tilde{a}^2mM^2u'^\ell_{(4)}}{\Lambda r^4}\,,
\tag{A7}
$$

$$
\tilde{A}^{(2)}_\ell = 0\,,
\tag{A8}
$$

$$
B^{(0)}_\ell = \frac{\tilde{a}^2mM^2\omega u^\ell_{(4)}}{\ell(\ell+1)r^3(2M-r)}-\frac{2\tilde{a}M^2\left((r-2M)u'^\ell_{(4)}+r^2\omega^2u^\ell_{(4)}\right)}{\Lambda r^4(2M-r)}\,,
\tag{A9}
$$

$$
B^{(1)}_\ell = \frac{i\tilde{a}^2mM^2u'^\ell_{(4)}}{\ell(\ell+1)r^3(2M-r)}-\frac{2i\tilde{a}M^2\omega u'^\ell_{(4)}}{\Lambda r^2(2M-r)}\,,
\tag{A10}
$$

$$
B^{(2)}_\ell = \frac{2i\tilde{a}^2mM^2ru^\ell_{(4)}}{\Lambda(r-2M)}-\frac{4i\tilde{a}M^2r^2\omega u^\ell_{(4)}}{\Lambda(r-2M)}\,,
\tag{A11}
$$

$$
\tilde{B}^{(0)}_\ell = \frac{4\tilde{a}^2M^3(\Lambda u^\ell_{(1)}+ir\omega u^\ell_{(3)})}{\ell(\ell+1)r^6}\,,
\tag{A12}
$$

$$
\tilde{B}^{(1)}_\ell = \frac{2\tilde{a}^2M^2\left((r-2M)u'^\ell_{(3)}-\Lambda u^\ell_{(2)}\right)}{\Lambda r^4(2M-r)}\,,
\tag{A13}
$$

$$
\tilde{B}^{(2)}_\ell = 0\,,
\tag{A14}
$$

$$D_\ell^{(0)} = \frac{\tilde{a}^2M^2}{r^6(2M-r)}\left[-(2M-r)(6M-\Lambda r)u^\ell_{(1)} + r\left((2M-r)\left(6Mu'^\ell_{(1)} - r(r-2M)u''^\ell_{(1)} + ir\omega\left(u^\ell_{(3)} - ru'^\ell_{(2)}\right)\right)\right.\right.$$
$$\left.\left. -ir\omega(10M-r)u^\ell_{(2)}\right)\right], \tag{A15}$$

$$D_\ell^{(1)} = \frac{\tilde{a}^2M^2}{r^4(r-2M)^2}\left[u^\ell_{(2)}\left(-\ell(\ell+1)(2M-r) - 2Mr^2\omega^2\right) + (2M-r)\left((r-2M)u'^\ell_{(3)} - 2iMr\omega u'^\ell_{(1)}\right) + 2iM\omega(2M-r)u^\ell_{(1)}\right], \tag{A16}$$

$$D_\ell^{(2)} = \frac{2\tilde{a}^2M^2}{2M-r}\left[-(2M-r)\left(ru'^\ell_{(2)} + u^\ell_{(2)} - {u_{(3)}}^\ell(r)\right) + 2iMr\omega u^\ell_{(1)}\right], \tag{A17}$$

and

$$\alpha_\ell = \frac{\tilde{a}^2M^2}{2\Lambda r^4(r-2M)^2}\left[-48M^3u'^\ell_{(3)} + 4M^2r\ell^2u'^\ell_{(2)} + 4\ell M^2ru'^\ell_{(2)} + 48M^2ru'^\ell_{(3)} - 4Mr^3\omega^2u^\ell_{(3)} + i\Lambda r^2\omega(2M+r)u^\ell_{(1)}\right.$$
$$-4Mr^2\ell^2u'^\ell_{(2)} - 4\ell Mr^2u'^\ell_{(2)} - 12Mr^2u'^\ell_{(3)} - 3\Lambda(r-2M)^2u^\ell_{(2)} + 4Mr(r-2M)^2u''^\ell_{(3)} + r^3\ell^2u'^\ell_{(2)} + \ell r^3u'^\ell_{(2)}\Big]$$
$$+\frac{2\tilde{a}mM^2(r\omega u^\ell_{(3)} - i\Lambda u^\ell_{(1)})}{\ell(\ell+1)r^3(2M-r)} + \frac{1}{\Lambda r^2(2M-r)}\left[4M^2u'^\ell_{(3)} - 2\mu^2Mr^2u^\ell_{(3)} - 2Mr\ell^2u'^\ell_{(2)} - 2\ell Mru'^\ell_{(2)} + \Lambda(2M-r)u^\ell_{(2)}\right.$$
$$\left.-2Mru'^\ell_{(3)} - r(r-2M)^2u''^\ell_{(3)} + \mu^2r^3u^\ell_{(3)} - r^3\omega^2u^\ell_{(3)} + i\Lambda r^2\omega u^\ell_{(1)} + r^2\ell^2u'^\ell_{(2)} + \ell r^2u'^\ell_{(2)}\right], \tag{A18}$$

$$\beta_\ell = \frac{\tilde{a}^2M^2\left(-u^\ell_{(4)}\left(\ell(\ell+1)(r-2M)^2 - 2Mr^3\omega^2\right) - 2M(r-2M)^2\left(ru''^\ell_{(4)} - 3u'^\ell_{(4)}\right)\right)}{\Lambda r^4(r-2M)^2} - \frac{2\tilde{a}mM^2\omega u^\ell_{(4)}}{\Lambda r^2(2M-r)}$$
$$+\frac{u^\ell_{(4)}\left((2M-r)\left(\Lambda+\mu^2r^2\right) + r^3\omega^2\right) + (2M-r)\left(r(2M-r)u''^\ell_{(4)} - 2Mu'^\ell_{(4)}\right)}{\Lambda r^2(2M-r)}, \tag{A19}$$

$$\zeta_\ell = -\frac{\tilde{a}^2mM^2\left(2\Lambda Mr\omega u^\ell_{(1)} - i\left(-2Mr^2\omega^2u^\ell_{(3)} + (r-2M)\left(-8Mu'^\ell_{(3)} - r(r-2M)u''^\ell_{(3)} + \Lambda ru'^\ell_{(2)}\right) + \Lambda(8M-r)u^\ell_{(2)}\right)\right)}{\Lambda r^4(2M-r)}$$
$$-\frac{6\tilde{a}M^2\left((2M-r)u^\ell_{(1)} + r\left((r-2M)u'^\ell_{(1)} + ir\omega u^\ell_{(2)}\right)\right)}{r^4(2M-r)}, \tag{A20}$$

$$\eta_\ell = \frac{2i\tilde{a}M^2\omega u^\ell_{(4)}}{2Mr^2-r^3} - \frac{i\tilde{a}^2mM^2\left(-2\left(6M^2-5Mr+r^2\right)u'^\ell_{(4)} + 2M\left(\Lambda+r^2\omega^2\right)u^\ell_{(4)} + r(r-2M)^2u''^\ell_{(4)}\right)}{\Lambda r^4(2M-r)}, \tag{A21}$$

$$\rho_\ell = \frac{\tilde{a}^2M^2}{\Lambda r^4(2M-r)}\left[12M^2u'^\ell_{(3)} - 2Mr^2\omega^2u^\ell_{(3)} + 2i\Lambda Mr\omega u^\ell_{(1)} - 2Mr\ell^2u'^\ell_{(2)} - 2\ell Mru'^\ell_{(2)} + 3\Lambda(2M-r)u^\ell_{(2)}\right.$$
$$\left.-10Mru'^\ell_{(3)} - r(r-2M)^2u''^\ell_{(3)} + r^2\ell^2u'^\ell_{(2)} + \ell r^2u'^\ell_{(2)} + 2r^2u'^\ell_{(3)}\right], \tag{A22}$$

$$\lambda_\ell = -\frac{4\tilde{a}^2M^3u^\ell_{(4)}}{r^5}, \tag{A23}$$

$$\sigma_\ell = 0, \tag{A24}$$

$$\gamma_\ell = \frac{\tilde{a}^2M^2}{\Lambda r^4(2M-r)}\left[u^\ell_{(4)}\left(\ell(\ell+1)(2M-r) + 2Mr^2\omega^2\right) + (2M-r)\left(r(2M-r)u''^\ell_{(4)} - 8Mu'^\ell_{(4)}\right)\right]. \tag{A25}$$

(A26)

Appendix B: Proca equation for a slowly rotating Kerr BH

In this Appendix we list the perturbation equations for a Proca field on a slowly rotating Kerr background to first order in $\tilde{a}$. Equation (55) reads

$$\hat{\mathcal{D}}_2u^\ell_{(4)} - \frac{4\tilde{a}M^2m\omega}{r^3}u^\ell_{(4)}$$
$$= \frac{6\tilde{a}M^2}{r^4}\left[(\ell+1)\mathcal{Q}_\ell\left(Fu^{\ell-1}_{(1)} - \mathrm{i}\,r\omega u^{\ell-1}_{(2)} - Fru'^{\ell-1}_{(1)}\right)\right.$$
$$\left.+\ell\mathcal{Q}_{\ell+1}\left(\mathrm{i}\,r\omega u^{\ell+1}_{(2)} - Fu^{\ell+1}_{(1)} + Fru'^{\ell+1}_{(1)}\right)\right], \tag{B1}$$

where the operator $\hat{\mathcal{D}}_2$ is defined in Eq. (24). The Lorenz condition (Eq. (53) with $I=2$) becomes

$$\begin{aligned}&\mathrm{i}\, r\omega u^{\ell}_{(1)} + F\left(u^{\ell}_{(2)} - u^{\ell}_{(3)} + r u'^{\ell}_{(2)}\right)\\ &-\frac{2\tilde{a}M^2 m}{r^2}\left(\mathrm{i}\, u^{\ell}_{(1)} + \frac{r\omega}{\Lambda}u^{\ell}_{(3)}\right)\\ &= \frac{2\mathrm{i}\,\tilde{a}M^2\omega}{r\Lambda}\left[(\ell+1)\mathcal{Q}_{\ell}u^{\ell-1}_{(4)} - \ell\mathcal{Q}_{\ell+1}u^{\ell+1}_{(4)}\right]. \qquad \text{(B2)}\end{aligned}$$

Using Eq. (B2), Eqs. (53) with $I=0,1$ and Eq. (54) read

$$\begin{aligned}&\hat{\mathcal{D}}_2 u^{\ell}_{(3)} + \frac{2F\ell(\ell+1)}{r^2}u^{\ell}_{(2)} + \frac{2\tilde{a}M^2 m}{r^4}\Big[r\omega(3u^{\ell}_{(2)} - 2u^{\ell}_{(3)})\\ &+3\mathrm{i}\, F\left(u^{\ell}_{(1)} - r u'^{\ell}_{(1)}\right)\Big] = 0\,, \qquad \text{(B3)}\\ &\hat{\mathcal{D}}_2 u^{\ell}_{(2)} - \frac{2F}{r^2}\left(1-\frac{3M}{r}\right)\left[u^{\ell}_{(2)} - u^{\ell}_{(3)}\right]\\ &-\frac{2\tilde{a}M^2 m}{\ell(\ell+1)r^4}\left[\ell(\ell+1)(2r\omega u^{\ell}_{(2)} - 3\mathrm{i}\, F u^{\ell}_{(1)}) - 3r\omega F u^{\ell}_{(3)}\right]\\ &= -\frac{6\mathrm{i}\,\tilde{a}M^2 F\omega}{\ell(\ell+1)r^3}\left[(\ell+1)\mathcal{Q}_{\ell}u^{\ell-1}_{(4)} - \ell\mathcal{Q}_{\ell+1}u^{\ell+1}_{(4)}\right], \qquad \text{(B4)}\\ &\hat{\mathcal{D}}_2 u^{\ell}_{(1)} - \frac{2M}{r^2}\left(\mathrm{i}\,\omega u^{\ell}_{(2)} + F u'^{\ell}_{(1)}\right)\\ &-\frac{2\tilde{a}M^2 m}{\ell(\ell+1)r^4}\left[\ell(\ell+1)(2r\omega u^{\ell}_{(1)} - \mathrm{i}\, u^{\ell}_{(2)}) + \mathrm{i}\, r F u'^{\ell}_{(3)}\right]\\ &= -\frac{2\tilde{a}M^2 F}{\ell(\ell+1)r^4}\Big[(\ell+1)\mathcal{Q}_{\ell}\left(2\ell u^{\ell-1}_{(4)} + r u'^{\ell-1}_{(4)}\right)\\ &+\ell\mathcal{Q}_{\ell+1}\left(2(\ell+1)u^{\ell+1}_{(4)} - r u'^{\ell+1}_{(4)}\right)\Big]. \qquad \text{(B5)}\end{aligned}$$

The system (B1), (B3)–(B5) can be greatly simplified by a systematic use of Eq. (B2) to eliminate $u^{\ell}_{(1)}$ and $u^{\ell\pm1}_{(1)}$. Solving Eq. (B2) for $u^{\ell}_{(1)}$ and substituting in Eq. (B3)–(B4) we get, to first order in $\tilde{a}$, the equations listed in the main text, namely Eqs.(59) and (60).

In order to simplify the axial equation (B1), we consider Eq. (B2) with $\ell-1$ and $\ell+1$ and solve it for $u^{\ell-1}_{(1)}$ and $u^{\ell+1}_{(1)}$, respectively. To first order in $\tilde{a}$, and making also use of Eq. (59) and (60), we get Eq. (61).

Appendix C: Analytical results for the axial modes

In this appendix we generalize Detweiler's calculation [60] of the unstable massive scalar modes of a Kerr BH to the case of a massive vector field. We focus on the axial sector and, unlike Detweiler, we work in the slow-rotation limit up to first order in $\tilde{a}$.

As discussed in the main text, the axial vector equation (65) and the equation for scalar perturbations (66) can be written in a unified form, Eq. (66). Thus, in order to include both scalar and axial vector perturbations, we shall solve Eq. (66) in the Kerr case, where $F = B = 1-2M/r$ and $\varpi = 2\tilde{a}M^2/r$. By defining $R(r) = \Psi/r$ we get

$$\begin{aligned}&r^2 F\frac{d}{dr}\left(r^2 F\frac{dR}{dr}\right) + \big[r^4\omega^2 - 4\tilde{a}mr\omega\\ &-r^2 F\left(\ell(\ell+1) + \mu^2 r^2 - \frac{2Ms^2}{r}\right)\Big]R = 0\,. \qquad \text{(C1)}\end{aligned}$$

For $s=0$, the equation above is equivalent to Eq. (7) in Ref. [60] at first order. For $s=\pm1$ and $\tilde{a}=0$ it is equivalent to Eq. (51) in Ref. [16].

Following Starobinski's method of matching asymptotics [92], we first expand Eq. (C1) for $r \gg M$:

$$\frac{d^2(rR)}{dr^2}\left[\omega^2 - \mu^2 + \frac{2M\mu^2}{r} - \frac{\ell(\ell+1)}{r^2}\right]rR = 0\,. \qquad \text{(C2)}$$

The solution of this equation with the correct boundary condition at infinity reads

$$R_{\infty}(x) \propto x^{\ell}e^{-x/2}U(\ell+1-\nu, 2\ell+2, x)\,, \qquad \text{(C3)}$$

where $U(p,q,x)$ is one of the confluent hypergeometric functions [93], $x = 2k_{\infty}r$, $k^2_{\infty} = \mu^2 - \omega^2$ and $\nu = M\mu^2/k_{\infty}$. The small distance ($x \ll 1$) behavior of the solution above reads

$$\begin{aligned}R_{\infty}(r) \sim (-1)^n\frac{(2\ell+1+n)!}{(2\ell+1)!}(2k_{\infty}r)^{\ell}\\ + (-1)^{n+1}\delta\nu(2\ell)!(2k_{\infty}r)^{-\ell-1}\,, \qquad \text{(C4)}\end{aligned}$$

where we have defined $\delta\nu = \nu - \ell - 1 - n$ and assumed $\delta\nu \sim x^{2\ell+1} \ll 1$ [60].

On the other hand, Eq. (C1) can be solved analytically also when $r \ll \max(\ell/\omega, \ell/\mu)$. In this limit, by introducing a new coordinate $z = (r-r_+)/r_+$, the equation reduces to

$$Z\frac{d}{dz}\left[Z\frac{dR}{dz}\right] + \left[P^2 - \ell(\ell+1)Z + s^2 z\right]R = 0\,. \qquad \text{(C5)}$$

We defined $Z = z(z+1)$ and

$$P = -2Mk_H = -2M(\omega - m\Omega_H)\,, \qquad \text{(C6)}$$

and we neglected $\mathcal{O}(\tilde{a}^2)$ terms in P^2. The general solution of Eq. (C5) is a combination of hypergeometric functions. By imposing ingoing waves at the horizon, i.e. $R \sim z^{iP}$ at $z \sim 0$, we get the general solution with the correct boundary condition:

$$\begin{aligned}R_H(r) \propto\, & e^{-2P\pi}(-1)^{2iP}z^{iP} \times\\ & {}_2F_1\left[-\ell + \mathrm{i}\, P + \sigma, 1 + \ell + \mathrm{i}\, P + \sigma, 1 + 2iP, -z\right],\end{aligned}$$

where ${}_2F_1(a,b,c,z)$ is the hypergeometric function [93] and $\sigma = \sqrt{s^2 - P^2}$. The large-distance limit of the equation above reads

$$\begin{aligned}R_H(r) \sim &\left[\frac{(2M)^{-\ell}\Gamma[1+2\ell]}{\Gamma\left[1+\ell+\mathrm{i}\, P-\sigma\right]\Gamma\left[1+\ell+\mathrm{i}\, P+\sigma\right]}\right]r^{\ell}\\ &+\left[\frac{(2M)^{1+\ell}\Gamma[-1-2\ell]}{\Gamma\left[-\ell+\mathrm{i}\, P-\sigma\right]\Gamma\left[-\ell+\mathrm{i}\, P+\sigma\right]}\right]r^{-\ell-1}\,. \qquad \text{(C7)}\end{aligned}$$

The key point of the method of matching asymptotics is that, when $|M\omega| \ll \ell$ and $M\mu \ll \ell$, there exists an overlapping region where Eqs. (C7) and (C4) are both valid. By equating the coefficients of r^ℓ and $r^{-\ell-1}$ one can fix the ratio of the overall factors and the frequency of the mode. Finally, we get

$$\delta\nu = \frac{(4k_\infty M)^{2\ell+1}\Gamma[-1-2\ell]\Gamma[2+n+2\ell]}{\Gamma[1+n]\Gamma[1+2\ell]^2\Gamma[2+2\ell]} \times \frac{\Gamma\left[1+iP-\sigma+\ell\right]\Gamma\left[1+\mathrm{i}\,P+\sigma+\ell\right]}{\Gamma\left[iP-\sigma-\ell\right]\Gamma\left[iP+\sigma-\ell\right]}\,. \tag{C8}$$

As in the case of massive scalar perturbations, the real and imaginary parts of the mode are related to μ and $\delta\nu$ by [60]

$$\mu^2 - \omega_R^2 = \mu^2\left(\frac{M\mu}{\ell+n+1}\right)^2\,, \tag{C9}$$

$$\mathrm{i}\,\omega_I = \frac{\delta\nu}{M}\left(\frac{M\mu}{\ell+n+1}\right)^3\,. \tag{C10}$$

In the slow-rotation limit we can further simplify Eq. (C8). To first order in P we get

$$\delta\nu \sim \frac{iP(4k_\infty M)^{2\ell+1}\Gamma[2+2\ell+n]}{\Gamma[1+2\ell]^2\Gamma[2+2\ell]^2\Gamma[1+n]} \times \Gamma[1+\ell-s]\Gamma[1+\ell+s]\Gamma[1+\ell]^2\prod_{j=1}^{s}\left[\frac{j-1-s-\ell}{s-j-\ell}\right]\,, \tag{C11}$$

When $s=0$ we recover the result for the scalar case [60] to first order in P (but see the subsection below for a discussion). In addition, our results correctly reduce to those found in Ref. [16] in the nonrotating limit. We can now evaluate the instability timescale. The fundamental mode reads

$$M\omega_I^{(\ell=1)} = \frac{(s+1)!(s+1)}{48}\left(\tilde{a}m - 2r_+\mu\right)(M\mu)^9\,, \tag{C12}$$

$$M\omega_I^{(\ell=2)} = \frac{\left[(2-s)!(2+s)!\right]^2}{885735}\left(\tilde{a}m - 2r_+\mu\right)(M\mu)^{13}\,,$$

for $\ell=1$ and $\ell=2$, respectively. Note that $\omega_I \sim \mu^{4\ell+5}$ for any value of s, so the only difference arises in the prefactor. We find

$$\frac{\omega_I^{(s=\pm1)}}{\omega_I^{(s=0)}} = \frac{(1+\ell)^2}{\ell^2}\,, \tag{C13}$$

which is independent of μ, $\tilde{a}$ and n. The instability timescale of the $\ell=1$ axial vector mode is 4 times shorter than that of the scalar mode. Equation (C12) is compared to the numerical results in Fig. 5.

On the analytical result in the massive scalar case

Although this is not directly related to the Proca problem, we wish to remark that when $s=0$ our equation (C11) differs from Eq. (28) in Ref. [60] (expanded at first order) by a factor 2 for any ℓ and any n. We believe this is either due to an inconsistent limit (explained below) or to a typo in Ref. [60] which propagates from Eqs. (21)-(24) to Eq. (25), where a factor 1/2 is missing. Thus, Eq. (29) in Detweiler should read $\gamma = \mu\tilde{a}(\mu M)^8/48$ for consistency with our Eq. (C12).

In order to understand the source of this discrepancy we refer the reader to the work by Furuhashi and Nambu [94], who extended Detweiler's calculation to the case of Kerr-Newman BHs, reproducing the results of Ref. [60] in the zero-charge limit. Ref. [94] presents a detailed derivation of the instability timescale, facilitating intermediate comparisons with our own calculation. We note that the results in Ref. [94] seem to be partially flawed because the limit defined in Eq. (23) in Ref. [94], $\Gamma(-n)/\Gamma(-m) = (-1)^{n-m}m!/n!$, is valid only when n and m are integers. However, in a rotating background the angular eigenvalues are not (in general) integers. For example, in the scalar case the separation constant $\lambda = \ell(\ell+1) + \mathcal{O}(\tilde{a}M\omega)$ [60]. In the $M\omega \ll 1$ limit, this can be accounted for by considering $\ell \to \ell+\epsilon$, with $\epsilon \ll 1$. When $s=0$, the evaluation of Eq. (C8) above involves limits of the form

$$\lim_{\epsilon\to0}\frac{\Gamma(-2\ell-2\epsilon-1)}{\Gamma(-\ell-\epsilon)} = \frac{(-1)^{\ell+1}}{2}\frac{\ell!}{(2\ell+1)!}\,, \tag{C14}$$

which differs by a factor 2 from Eq. (23) in Ref. [94] (see also the discussion in Ref. [95]). We believe that this is the reason for our factor 2 discrepancy with respect to Furuhashi and Nambu (and presumably also with respect to Detweiler's calculation). Despite numerical difficulties in the $M\mu \ll 1$ limit, our numerical calculations for $\ell = m = 1$ are in better agreement with a prefactor of 1/48, as computed in Eq. (C12): see also Sec. VI F and Fig. 6 in Ref. [35].

[1] H.-P. Nollert, Class.Quant.Grav. **16**, R159 (1999).

[2] K. D. Kokkotas and B. G. Schmidt, Living Rev.Rel. **2**, 2 (1999), arXiv:gr-qc/9909058 [gr-qc].

[3] V. Ferrari and L. Gualtieri, Gen.Rel.Grav. **40**, 945 (2008), arXiv:0709.0657 [gr-qc].

[4] E. Berti, V. Cardoso, and A. O. Starinets,

Class.Quant.Grav. **26**, 163001 (2009), arXiv:0905.2975 [gr-qc].
[5] R. Konoplya and A. Zhidenko, Rev.Mod.Phys. **83**, 793 (2011), arXiv:1102.4014 [gr-qc].
[6] P. Amaro-Seoane, J. R. Gair, M. Freitag, M. Coleman Miller, I. Mandel, *et al.*, Class.Quant.Grav. **24**, R113 (2007), arXiv:astro-ph/0703495 [ASTRO-PH].
[7] L. Barack, Class.Quant.Grav. **26**, 213001 (2009), arXiv:0908.1664 [gr-qc].
[8] E. Poisson, A. Pound, and I. Vega, Living Rev.Rel. **14**, 7 (2011), arXiv:1102.0529 [gr-qc].
[9] E. Berti, V. Cardoso, J. A. Gonzalez, U. Sperhake, M. Hannam, *et al.*, Phys.Rev. **D76**, 064034 (2007), arXiv:gr-qc/0703053 [GR-QC].
[10] E. Berti, V. Cardoso, T. Hinderer, M. Lemos, F. Pretorius, *et al.*, Phys.Rev. **D81**, 104048 (2010), arXiv:1003.0812 [gr-qc].
[11] V. Cardoso, L. Gualtieri, C. Herdeiro, U. Sperhake, P. M. Chesler, *et al.*, (2012), arXiv:1201.5118 [hep-th].
[12] S. Chandrasekhar, *The mathematical theory of black holes* (Oxford University Press, New York, 1992).
[13] S. A. Teukolsky, Astrophys.J. **185**, 635 (1973).
[14] M. Durkee and H. S. Reall, Class.Quant.Grav. **28**, 035011 (2011), arXiv:1009.0015 [gr-qc].
[15] G. Torres del Castillo and G. Silva-Ortigoza, Phys.Rev. **D42**, 4082 (1990).
[16] J. G. Rosa and S. R. Dolan, Phys.Rev. **D85**, 044043 (2012), arXiv:1110.4494 [hep-th].
[17] Y. Kojima, Phys.Rev. **D46**, 4289 (1992).
[18] Y. Kojima, Astrophys.J. **414**, 247 (1993).
[19] Y. Kojima, Progress of Theoretical Physics **90**, 977 (1993).
[20] M. Bruni, L. Gualtieri, and C. F. Sopuerta, Class.Quant.Grav. **20**, 535 (2003), arXiv:gr-qc/0207105 [gr-qc].
[21] S. Chandrasekhar and V. Ferrari, Proc.Roy.Soc.Lond. **A433**, 423 (1991).
[22] N. Yunes and F. Pretorius, Phys.Rev. **D79**, 084043 (2009), arXiv:0902.4669 [gr-qc].
[23] K. Konno, T. Matsuyama, and S. Tanda, Prog.Theor.Phys. **122**, 561 (2009), arXiv:0902.4767 [gr-qc].
[24] P. Pani and V. Cardoso, Phys.Rev. **D79**, 084031 (2009), arXiv:0902.1569 [gr-qc].
[25] P. Pani, C. F. Macedo, L. C. Crispino, and V. Cardoso, Phys.Rev. **D84**, 087501 (2011), arXiv:1109.3996 [gr-qc].
[26] K. Yagi, N. Yunes, and T. Tanaka, Phys.Rev. **D86**, 044037 (2012), arXiv:1206.6130 [gr-qc].
[27] N. Andersson, Astrophys.J. **502**, 708 (1998), arXiv:gr-qc/9706075 [gr-qc].
[28] Y. Kojima, Mon.Not.Roy.Astron.Soc. **293**, 49 (1998), arXiv:gr-qc/9709003 [gr-qc].
[29] K. H. Lockitch and J. L. Friedman, Astrophys.J. **521**, 764 (1999), arXiv:gr-qc/9812019 [gr-qc].
[30] K. H. Lockitch, N. Andersson, and J. L. Friedman, Phys.Rev. **D63**, 024019 (2001), arXiv:gr-qc/0008019 [gr-qc].
[31] W. H. Press and S. A. Teukolsky, Nature **238**, 211 (1972).
[32] T. Damour, N. Deruelle, and R. Ruffini, Lett.Nuovo Cim. **15**, 257 (1976).
[33] V. Cardoso, O. J. Dias, J. P. Lemos, and S. Yoshida, Phys.Rev. **D70**, 044039 (2004), arXiv:hep-th/0404096 [hep-th].
[34] V. Cardoso and S. Yoshida, JHEP **0507**, 009 (2005), arXiv:hep-th/0502206 [hep-th].
[35] S. R. Dolan, Phys.Rev. **D76**, 084001 (2007), arXiv:0705.2880 [gr-qc].
[36] J. Rosa, JHEP **1006**, 015 (2010), arXiv:0912.1780 [hep-th].
[37] V. Cardoso, S. Chakrabarti, P. Pani, E. Berti, and L. Gualtieri, Phys.Rev.Lett. **107**, 241101 (2011), arXiv:1109.6021 [gr-qc].
[38] T. Zouros and D. Eardley, Annals Phys. **118**, 139 (1979).
[39] S. Hawking, Mon.Not.Roy.Astron.Soc. **152**, 75 (1971).
[40] Y. B. Zel'Dovich and I. D. Novikov, Astron.Zh. **43**, 758 (1966).
[41] B. J. Carr and S. W. Hawking, Mon.Not.Roy.Astron.Soc. **168**, 399 (1974).
[42] A. Arvanitaki, S. Dimopoulos, S. Dubovsky, N. Kaloper, and J. March-Russell, Phys.Rev. **D81**, 123530 (2010), arXiv:0905.4720 [hep-th].
[43] A. Arvanitaki and S. Dubovsky, Phys.Rev. **D83**, 044026 (2011), arXiv:1004.3558 [hep-th].
[44] N. Yunes, P. Pani, and V. Cardoso, Phys.Rev. **D85**, 102003 (2012), arXiv:1112.3351 [gr-qc].
[45] J. Alsing, E. Berti, C. M. Will, and H. Zaglauer, Phys.Rev. **D85**, 064041 (2012), arXiv:1112.4903 [gr-qc].
[46] H. Kodama and H. Yoshino, (2011), arXiv:1108.1365 [hep-th].
[47] H. Yoshino and H. Kodama, Prog.Theor.Phys. **128**, 153 (2012), arXiv:1203.5070 [gr-qc].
[48] G. Mocanu and D. Grumiller, Phys.Rev. **D85**, 105022 (2012), arXiv:1203.4681 [astro-ph.CO].
[49] M. Goodsell, J. Jaeckel, J. Redondo, and A. Ringwald, JHEP **0911**, 027 (2009), arXiv:0909.0515 [hep-ph].
[50] J. Jaeckel and A. Ringwald, Ann.Rev.Nucl.Part.Sci. **60**, 405 (2010), arXiv:1002.0329 [hep-ph].
[51] P. G. Camara, L. E. Ibanez, and F. Marchesano, JHEP **1109**, 110 (2011), arXiv:1106.0060 [hep-th].
[52] A. S. Goldhaber and M. M. Nieto, Rev.Mod.Phys. **82**, 939 (2010), arXiv:0809.1003 [hep-ph].
[53] D. Gal'tsov, G. Pomerantseva, and G. Chizhov, Sov.Phys.J. **27**, 697 (1984).
[54] C. Herdeiro, M. O. Sampaio, and M. Wang, Phys.Rev. **D85**, 024005 (2012), arXiv:1110.2485 [gr-qc].
[55] R. Konoplya, Phys.Rev. **D73**, 024009 (2006), arXiv:gr-qc/0509026 [gr-qc].
[56] L. Brenneman, C. Reynolds, M. Nowak, R. Reis, M. Trippe, *et al.*, Astrophys.J. **736**, 103 (2011), arXiv:1104.1172 [astro-ph.HE].
[57] S. Schmoll, J. Miller, M. Volonteri, E. Cackett, C. Reynolds, *et al.*, Astrophys.J. **703**, 2171 (2009), arXiv:0908.0013 [astro-ph.HE].
[58] E. Leaver, Proc.Roy.Soc.Lond. **A402**, 285 (1985).
[59] P. Pani, V. Cardoso, L. Gualtieri, E. Berti, and A. Ishibashi, (2012), to appear in Physical Review Letters.
[60] S. L. Detweiler, Phys. Rev. **D22**, 2323 (1980).
[61] `http://blackholes.ist.utl.pt/?page=Files`, `http://www.phy.olemiss.edu/~berti/qnms.html`.
[62] J. B. Hartle, Astrophys.J. **150**, 1005 (1967).
[63] V. Ferrari, L. Gualtieri, and S. Marassi, Phys.Rev. **D76**, 104033 (2007), arXiv:0709.2925 [gr-qc].
[64] E. Berti, V. Cardoso, and M. Casals, Phys.Rev. **D73**, 024013 (2006), arXiv:gr-qc/0511111 [gr-qc].
[65] U. Gerlach and U. Sengupta, Phys.Rev. **D22**, 1300 (1980).
[66] S. Teukolsky and W. Press, Astrophys.J. **193**, 443 (1974).

[67] E. Berti, F. White, A. Maniopoulou, and M. Bruni, Mon.Not.Roy.Astron.Soc. **358**, 923 (2005), arXiv:gr-qc/0405146 [gr-qc].

[68] K. H. Lockitch and N. Andersson, Class.Quant.Grav. **21**, 4661 (2004), arXiv:gr-qc/0106088 [gr-qc].

[69] E. W. Leaver, Phys.Rev. **D41**, 2986 (1990).

[70] C. Simmendinger, A. Wunderlin, and A. Pelster, Phys. Rev. E **59**, 5344 (1999), arXiv:math-ph/0106011.

[71] K. S. Thorne, Astrophys. J. **158**, 1 (1969).

[72] S. Chandrasekhar and V. Ferrari, Proc.Roy.Soc.Lond. **A437**, 133 (1992).

[73] E. Berti, V. Cardoso, and P. Pani, Phys.Rev. **D79**, 101501 (2009), arXiv:0903.5311 [gr-qc].

[74] R. Ruffini, *Black Holes: les Astres Occlus* (Gordon and Breach Science Publishers, 1973).

[75] D. Merritt and M. Milosavljevic, Living Rev.Rel. **8**, 8 (2005), arXiv:astro-ph/0410364 [astro-ph].

[76] A. Sesana, F. Haardt, and P. Madau, Astrophys.J. **660**, 546 (2007), arXiv:astro-ph/0612265 [astro-ph].

[77] E. Barausse, Mon.Not.Roy.Astron.Soc. **423**, 2533 (2012), arXiv:1201.5888 [astro-ph.CO].

[78] E. Berti and M. Volonteri, Astrophys.J. **684**, 822 (2008), arXiv:0802.0025 [astro-ph].

[79] J. M. Bardeen, Nature **226**, 64 (1970).

[80] K. S. Thorne, Astrophys.J. **191**, 507 (1974).

[81] C. F. Gammie, S. L. Shapiro, and J. C. McKinney, Astrophys.J. **602**, 312 (2004), arXiv:astro-ph/0310886 [astro-ph].

[82] A. R. King and J. Pringle, Mon.Not.Roy.Astron.Soc.Lett. **373**, L93 (2006), arXiv:astro-ph/0609598 [astro-ph].

[83] R. Harnik, J. Kopp, and P. A. Machado, JCAP **1207**, 026 (2012), arXiv:1202.6073 [hep-ph].

[84] N. J. McConnell, C.-P. Ma, K. Gebhardt, S. A. Wright, J. D. Murphy, T. R. Lauer, J. R. Graham, and D. O. Richstone, Nature (London) **480**, 215 (2011), arXiv:1112.1078 [astro-ph.CO].

[85] N. J. McConnell, C.-P. Ma, J. D. Murphy, K. Gebhardt, T. R. Lauer, J. R. Graham, S. A. Wright, and D. O. Richstone, ArXiv e-prints (2012), arXiv:1203.1620 [astro-ph.CO].

[86] J. Beringer *et al.* (Particle Data Group), Phys.Rev. **D86**, 010001 (2012).

[87] H. A. Buchdahl, J.Phys.A **A12**, 1235 (1979).

[88] V. Vitagliano, T. P. Sotiriou, and S. Liberati, Phys.Rev. **D82**, 084007 (2010), arXiv:1007.3937 [gr-qc].

[89] H. Sotani, K. Kokkotas, and N. Stergioulas, Mon.Not.Roy.Astron.Soc. **375**, 261 (2007), arXiv:astro-ph/0608626 [astro-ph].

[90] A. Stavridis, A. Passamonti, and K. Kokkotas, Phys.Rev. **D75**, 064019 (2007), arXiv:gr-qc/0701122 [gr-qc].

[91] A. Passamonti, A. Stavridis, and K. Kokkotas, Phys.Rev. **D77**, 024029 (2008), arXiv:0706.0991 [gr-qc].

[92] A. A. Starobinsky, Zh. Eksp. Teor. Fiz **64**, 48 (1973), sov. Phys. JETP 37, 28 (1973).

[93] M. Abramowitz and I. A. Stegun, *Handbook of Mathematical Functions with Formulas, Graphs, and Mathematical Tables*, ninth dover printing, tenth gpo printing ed. (Dover, New York, 1964).

[94] H. Furuhashi and Y. Nambu, Prog.Theor.Phys. **112**, 983 (2004), arXiv:gr-qc/0402037 [gr-qc].

[95] J. G. Rosa, (2012), arXiv:1209.4211 [hep-th].